A DISSERTATION

FOR THE DEGREE OF DOCTOR OF PHILOSOPHY

Clinical Effectiveness of Strain Elastography Combined with Lymphosonography for Mandibular Lymph Node Assessment in Patients with Head and Neck Cancer Dogs

두경부 종양 개에서 탄성 초음파 및 초음파 림프조영을 이용한 하악 림프절 평가의 임상적 유용성

by

Mihyun Choi

MAJOR IN VETERINARY CLINICAL SCIENCES

DEPARTMENT OF VETERINARY MEDICINE

GRADUATE SCHOOL

SEOUL NATIONAL UNIVERSITY

August, 2020

Clinical Effectiveness of Strain Elastography Combined with Lymphosonography for Mandibular Lymph Node Assessment in Patients with Head and Neck Cancer Dogs

by
Mihyun Choi

Supervised by
Professor Mincheol Choi

A Dissertation submitted to
the Graduate School of Seoul National University
in partial fulfillment of the requirement
for the degree of Doctor of Philosophy in Veterinary Medicine
June, 2020

MAJOR IN VETERINARY CLINICAL SCIENCES
DEPARTMENT OF VETERINARY MEDICINE
GRADUATE SCHOOL
SEOUL NATIONAL UNIVERSITY
August, 2020

Clinical Effectiveness of Strain Elastography Combined with Lymphosonography for Mandibular Lymph Node Assessment in Patients with Head and Neck Cancer Dogs

Mihyun Choi

Supervised by

Professor Mincheol Choi

Major in Veterinary Clinical Sciences

Department of Veterinary Medicine

Graduate School of Seoul National University

ABSTRACT

Determining lymph node metastasis in tumor patients is important in assessing the staging and therapeutic plan. Multiple imaging techniques have been used to evaluate lymph nodes of cancer patient. However, there are overlapping results

between benign and malignant lymph nodes as well as cumbersome techniques. Therefore, noninvasive, simple, and accurate imaging techniques are required for pre-surgical assessment of patients with head and neck cancers.

Recently, lymphosonography and ultrasound elastography have been utilized to evaluate lymph nodes. Lymphosonography aids cytology/biopsy procedures or lymph node status through visualization of the lymphatic system. Strain elastography also provides diagnostic information, as metastatic nodes have greater stiffness than normal lymph nodes. However, the clinical usefulness of sonoelastography and lymphosonography has not yet been demonstrated in dogs. Therefore, the objectives of this study were to determine the normal reference ranges of mandibular lymph nodes on strain elastography for qualitative and semi-quantitative analysis (Chapter I), and to evaluate lymph nodes after injection of perflubutane microbubbles for lymphosonography (Chapter II) in clinically healthy dogs, and to evaluate the clinical applications of both methods on patient with head/neck cancer (Chapter III).

In Chapter I, 45 clinically healthy dogs were enrolled. Ultrasonographic elastographic images were evaluated qualitatively (elastographic pattern) and semi-quantitatively (mean hue histogram and stiffness area ratios). Elastographic patterns were classified into grades 1 to 4, according to the percentage of high elasticity by visualization. The mean hue histogram was defined as the mean pixel color values within the lymph node. Stiffness area ratios were determined by the stiff area, and the two criteria were evaluated using a computer program (Image J®). Clinically healthy mandibular lymph nodes exhibited predominantly red and green colors.

Upon elastographic pattern evaluation, all lymph nodes were graded 1 or 2 (1.23 ± 0.42, mean ± SD). The mean hue histogram values were 80.96 ± 8.29. The stiffness area ratios were 0.03 ± 0.02. The mean hue histogram, stiffness area ratio and elastographic pattern exhibited no correlation with age and showed moderate to excellent repeatability and reproducibility.

In Chapter II, 11 clinically healthy dogs were enrolled. The lymphosonographic images were evaluated quantitatively (the visualization of lymphatic vessels/lymph nodes (LN), contrast transit time and contrast enhancement intensity using Image J®) and qualitatively (enhancement pattern). On lymphosonography, the afferent lymphatic vessels (8/11) were hyperechoic linear structures leading from the injection site. The measured median (range) was 1.2 (0.7-1.8) *mm,* and these vessels could be readily traced to their mandibular LN (11/11). Normal lymphatic vessels were visualized within five mins post-injection, while the mandibular LN were identified after simultaneous enhancement with lymphatic vessels that lasted 10 mins post-injection. The median values of contrast enhancement intensity were 64.53 (range: 24.81-128.43). Capsular or completely filled enhancement was observed in clinically healthy LNs. Lymphosonography can be used to detect lymphatic drainage pathways.

In Chapter III, the above two methods were applied to patients with head/ neck cancer. Twenty-one lymph nodes (non-metastatic LN; *n*=8, metastatic LN; *n*=13) and eleven dogs (non-metastatic dogs; *n*=5, metastatic dogs; *n*=6) were enrolled for strain elastography and lymphosonography, respectively. On strain elastography, clinically

healthy (45/45) and non-metastatic(1/8) LN showed a homogeneous green color (soft), but metastatic LNs (12/13) tended to have a heterogenous blue color (stiffer). There were significant differences in the qualitative and quantitative strain elastographic criteria between the metastatic nodes and clinically healthy or non-metastatic nodes (p<0.05). Receiver operating characteristic curve (ROC) analyses revealed that cutoff values for the prediction of malignancy were 92.26 for the mean hue histogram (sensitivity: 100%, specificity: 92%), and 0.17 for stiffness area ratios (sensitivity: 86%, specificity of 100%). For lymphosonography, clinically healthy (11/11) and non-metastatic LN (4/5) showed a homogenous enhancement pattern with centripetal filling, whereas all metastatic LNs (6/6) showed a focal or complete filling defect. There was a significant difference in the qualitative and quantitative criteria for lymphosonographic contrast enhancement pattern (p<0.05). In addition, these two combined evaluations showed the highest AUC of 0.999 (95% CI, 0.999-1.000) compared to strain elastography or lymphosonography alone. Higher tissue stiffness and filling defects of metastatic lymph nodes might be associated with altered tissue composition and structure. For metastatic lymph nodes, the cortex was damaged and thickened with proliferation as well as cornification of cancer cells. These alterations may produce keratin/fibrin or destroy the small lymphatic vessels.

In conclusion, qualitative and semi-quantitative evaluations of strain elastography have the potential to predicting lymph node malignancy, and filling defects in lymphosonography highly indicates malignancy. However, when using strain elastography or lymphosonography alone, there were false positive or false

negative findings. Therefore, the combination of lymphosonography and strain elastography could be more useful for predicting malignancy of lymph nodes.

Keywords: Canine, head and neck cancer, mandibular lymph node, perflubutane microbubble, lymphosonography, semiquantitative strain elastography

Student number: 2015-31181

CONTENTS

LIST OF ABBREVIATION

AE phenomenon	Acoustic emission phenomenon
ANOVA	One-way analysis of variance
AUC	Area under the curve
BW	Body weight
CI	Confidence interval
CT	Computed tomography
ICC	Intra-class correlations
LN	Lymph node
Mean HH	Mean hue histogram values
NIR	Near-infrared fluorescence imaging
PACS	Picture Archiving and Communication System
r	Correlation coefficient
R^2	Coefficient of determination
RES	Reticulo-endothelial specific agent
ROC	Receiver operating characteristics
ROI	Region of interest
SAR	Stiffness area ratio
SD	Standard deviation

LIST OF FIGURES

LIST OF TABLES

GENERAL INTRODUCTION

Accurate staging is a cornerstone of oncologic management, guiding both prognosis and treatment options for patients. Solid tumors of the head occur commonly in veterinary oncology and lymph node metastasis is a frequent finding in oral malignancies (Herring *et al.*, 2002). While rates of lymphatic metastasis vary depending on tumor type, histologic grade, and location, an increased tumor stage has been identified as a negative prognostic factor for a range of neoplastic processes (Culp *et al*., 2013; Ciekot *et al*., 1994; Boston *et al.*, 2014; Fulton *et al.*, 2013; Proulx *et al.*, 2003; Williams *et al.*, 2003). Lymph node size alone has been shown to be a poor marker of the presence or absence of metastasis in dogs (Williams *et al.*, 2003; Langenbach *et al.*, 2001; Gieger *et al.*, 2003).

Multiple imaging techniques can also be used to detect abnormal lymph nodes (Nyman *et al.*, 2005; Nyman *et al.*, 2006; Nyman and O'Brien, 2007; Seiler and Griffith, 2018; Johnson *et al*., 2016; Ballegeer *et al*., 2010; Grimes *et al*., 2017; Stahle *et al*., 2018), However, there is an overlap of results, requirement for general anesthesia, and use of ionizing radiation in computed tomography between benign and malignant lymph nodes (Nyman *et al*., 2006; Nyman and O'Brien, 2007; Seiler and Griffith, 2018). Therefore, noninvasive and simple imaging techniques are required for pre-surgical assessment of patients with head and neck cancers.

The use of elastography or contrast-enhanced ultrasonography for differentiating between non-metastatic or metastatic lymph nodes has been reported recently. Elastography is an imaging modality used to map the elastic properties of

soft tissues (Tan *et al*., 2010). Malignant tissues tend to be stiffer than normal tissues as they contain an increased density of tumor cells, vasculature and fibrotic material (Bhatia *et al*., 2010; Tan *et al*., 2010). Given these properties, elastography has been used to assess various human organs for malignancy (Alam *et al.*, 2008; Bhatia *et al*., 2010; Tan *et al*., 2010). The successful use of strain elastography for qualitative analysis of lymph nodes has also been reported in veterinary medicine (Seiler and Griffith, 2018; Belotta *et al*., 2019). However, evaluation of mandibular lymph nodes using semi-quantitative elastography for predicting malignancy has not yet been reported in veterinary medicine.

Lymphosonography is a new technique for lymph node biopsy and lymphatic system evaluation that utilizes injection of contrast media to the parenchyma (Goldberg *et al*., 2004). The technique has only been used pre-clinically and tested in proof-of-concept studies mainly involving pigs, dogs, and rabbits to evaluate mammary gland tumors (Goldberg *et al*., 2005; Lurie *et al*., 2006; Curry et al., 2007; Gelb *et al*., 2010; Goldberg *et al*., 2011; Liu *et al*., 2014; Favril *et al*., 2019). They used a non-mononuclear phagocytic system agent (e.g., sulfur hexafluoride (SonoVue®)) and examined only axillary, inguinal, and popliteal lymph nodes. Furthermore, lymphosonography combined with strain elastography for lymph node evaluation was not reported in veterinary medicine.

Therefore, the purpose of this study was to determine normal imaging characteristics using strain elastography (Chapter I) and lymphosonography (Chapter II) in clinically healthy dogs and to apply these methods to patients with

head and neck cancer (Chapter III). In chapter I, the determined normal reference range of the mandibular lymph node was determined using qualitative and semi-quantitative strain elastography analysis. In chapter II, lymph nodes were evaluated after injection using a mononuclear phagocytic system-specific agent (perflubutane microbubbles, Sonazoid®). The hypothesis was that findings in clinically healthy, non-metastatic and metastatic lymph nodes showed differences upon lymphosonography and strain elastography.

CHAPTER I

Qualitative and semi-quantitative strain elastography of mandibular lymph node in clinically healthy dogs

INTRODUCTION

Assessment of regional lymph nodes is important for staging head and neck cancers, as well as for establishing prognosis (Herring *et al*., 2002). Although the rates of lymph node metastasis vary with tumor type, histologic grade, and location, increased tumor size has been identified as a global negative prognostic factor (Theon *et al*., 1997). Manual palpation of lymph nodes has generally been promoted in veterinary medicine. However, more than 85% of dogs with lymph node metastasis are not diagnosed (Brissot *et al*., 2017), since cytological or histopathological examination is required for accurate metastasis evaluation (Langenbach *et al*., 2001).

Multiple imaging techniques can also be used to detect abnormal lymph nodes (Nyman *et al*., 2006; Nyman and O'Brien, 2007; Seiler and Griffith, 2018; Johnson *et al*., 2016; Ballegeer *et al*., 2010; Grimes *et al*., 2017; Stahle *et al*., 2018). However, overlapping results between benign and malignant lymph nodes (Nyman *et al*., 2006; Nyman and O'Brien, 2007; Seiler and Griffith, 2018), the requirement for general anesthesia (Johnson *et al*., 2016; Ballegeer *et al*., 2010; Grimes *et al*., 2017; Stahle *et al*., 2018), and the use of ionizing radiation on computed tomography (Ballegeer

et al., 2010; Grimes *et al*., 2017), are critical limitations. Therefore, noninvasive and simple imaging techniques are required for the pre-surgical assessment of patients with head and neck cancers.

Elasticity is a mechanical tissue characteristic preventing tissue displacement under pressure (Ozturk *et al*., 2018, Dietrich and Cantisani 2014). It varies depending on the tissue type (fat, collagen, etc.) and tissue's pathologic status (inflammation, neoplasia) (Alam *et al*., 2008). In sonographic elastography, image representations of tissue hardness can be obtained using a conventional sonography machine with special software and a conventional ultrasound probe (Ophir *et al*., 1991). Elastography is an imaging modality used to map the elastic properties of soft tissues by which tissue stiffness is estimated as a physical property, termed the Young's modulus (E) (Bhatia *et al*., 2010). Young's modulus is a proportionality constant that relates the applied force per unit area or stress, and the resultant relative change in tissue dimension, or strain (Ozturk *et al*., 2018). Ultrasound elastography methods can be divided into two categories: strain and shear wave based. Strain elastography measures tissue stiffness by applying external tissue pressure (Ophir *et al*., 1991). Tissue dimensions change due to the applied pressure, with this deformation being termed as strain. Stiffer lesions deform less and have correspondingly lower strain and higher Young's modulus (Ophir *et al*., 1991). Parameters commonly used in strain elastography are as follows: strain ratio (Sigrist *et al*., 2017), elasticity scores (Shiina *et al*., 2015; Itoh *et al*., 2006), fat to lesion strain ratio (Zhou *et al*., 2014) and elastography-to B-mode size ratio (Barr *et al*., 2010). Shear wave elastography

(Sigrist *et al*., 2017) exploits the fact that shear waves propagate faster in hard versus soft tissue. Young's modulus can be algebraically derived from the shear wave speed (SWS). This can be qualitatively assessed by analyzing a color-scale image, and/or quantitively assessed by determining the maximum elasticity value (kPa). A color closer to the red end of the spectrum represents a higher kPa value indicating a stiffer tissue (Lee *et al*., 2014).

Ultrasound elastography is used in clinical practice based on the premise that pathological processes such as cancer modify the physical characteristics of diseased tissue. Malignant tissues tend to be stiffer than normal tissues as they contain an increased density of tumor cells, vasculature, and fibrotic material (Tan *et al*., 2010; Thomas *et al*., 2006; Burnside *et al*., 2007; Regner *et al*., 2006). Given these properties, elastography has been used to assess various human organs for malignancy (Bhatia *et al*., 2010; Tan *et al*., 2010; Thomas *et al*., 2006; Burnside *et al*., 2007; Regner *et al*., 2006; Desmots *et al*., 2016; Alam *et al*., 2008). The successful use of strain elastography for qualitative analysis of lymph nodes has also been reported in veterinary medicine (Seiler and Griffth, 2018; Belotta *et al*., 2019). However, to our knowledge, evaluation of mandibular lymph nodes using semi-quantitative elastography for predicting malignancy has not yet been reported in veterinary medicine.

Therefore, the aim of this study was to determine normal reference ranges of mandibular lymph nodes in cinically healthy dogs upon qualitative and semi-quantitative analysis on strain elastography, and the diagnostic accuracy and cutoff

values for predicting malignancy of mandibular lymph nodes. The hypothesis was that the results of strain elastography would differ between non-metastatic and metastatic lymph nodes.

MATERIALS AND METHODS

1. Animals

Client-owned dogs, presented to the Haemaru Referral Animal Hospital, Seoul, Korea were included in the study (September 2017-December 2018). The visiting purpose of these dogs was undergoing regular medical health examination. Owner consent was obtained and all of owners were participated voluntarily. Dogs were classified as clinical healthy based on routine physical examination, complete blood analysis (including complete blood count, biochemical profile and C-reactive protein level), radiologic examination (thoracic radiography and abdominal ultrasound) and the absence of any known malignancy and inflammation/infection.

2. Ultrasound procedure

2-1. Grey-scale ultrasonography

Examinations were performed by the first author using a 2-12 MHz linear probe (Arietta 60, Hitachi-Aloka, Tokyo, Japan) in lateral recumbency. The procedure was performed while the dogs were awake. Depth, gain, and focus were altered as needed to obtain optimal image quality. Image of the left mandibular lymph node were obtained longitudinal plane so that the maximal length, width of each lymph node could be recorded in centimeters. Length was measured as the longest dimension; width was the measurement perpendicular to length. If there was more than one lymph node present in a particular area, all lymph nodes were measured and recorded. The echogenicity of each lymph node was recorded relative to the adjacent fat as hypoechoic, hyperechoic or isoechoic, and the margin of each lymph nodes was recorded as either smooth or irregular.

2-2. Strain elastography

Strain elastography was performed in the same ultrasound unit. After acquiring a grey-scale ultrasonography image of the left mandibular lymph node in the longitudinal plane, a region of interest comprising the lymph node and surrounding tissue was selected. For strain elastography, compression with light pressure followed by decompression was applied repeatedly until a stable image was obtained. The direction of compression was upwards and then downwards. Real-time elastographic and B-mode images simultaneously appeared side-by-side on the screen. Regions-of-interest (ROIs) included the target lymph nodes, but no other tissues (e.g., bone, blood vessel) that may disturb analysis of the relative stiffness of the target lymph nodes. At least three elastographic images were obtained and these measurements were performed by two investigators independently for analysis of repeatability and reproducibility. In cases in which acquisition of uniform and regular movements was not feasible, nodes were excluded from the analysis.

All ultrasound elastographic images were displayed using 256-color mapping of each pixel according to the degree of strain with the color scale going from red (highest strain, softest) to, green (average strain, intermediate), to blue (no strain, hardest). All images were sent to a PACS (INFINITT, Infinitt Healthcare Co., Ltd., Seoul, South Korea) and were then saved as bit-map files for later analysis.

3. Image analysis

3-1. Grey scale ultrasonography

B-mode images were evaluated on the basis of size, shape of the lymph node, presence of the hyperechoic hilum, margin and echogenicity. The height of the lymph node (in *cm*) was evaluated to determine size. Length-to-width ratio was used to determine shape. The lymph node margins were classified as irregular or smooth. Lymph node echogenicity was classified as hypoechoic or isoechoic as compared to adjacent fat.

3-2. Strain elastography

3-2-1. Qualitative analysis

Strain elastographic images were evaluated qualitatively and semi-quantitatively. If an anechoic structure (suspected cystic or necrotic changes) was found in the parenchyma, it was not included in the analysis because these are not indicative of a solid component. In those cases, the remain parenchyma was evaluated. For qualitative analysis, the elastographic patterns were classified based on the distribution and percentage of the lymph node area to the hardness area (blue), subjectively (Figure 1) (Alam *et al*., 2008).

1. Grade 1 indicated absent or very low stiffness (i.e., blue)
2. Grade 2 indicated a stiff area comprising < 50% of the lymph node
3. Grade 3 indicated a stiff area comprising > 50% of the lymph node
4. Grade 4 indicated a lymph node with predominant stiffness that occupied the entire lymph node space

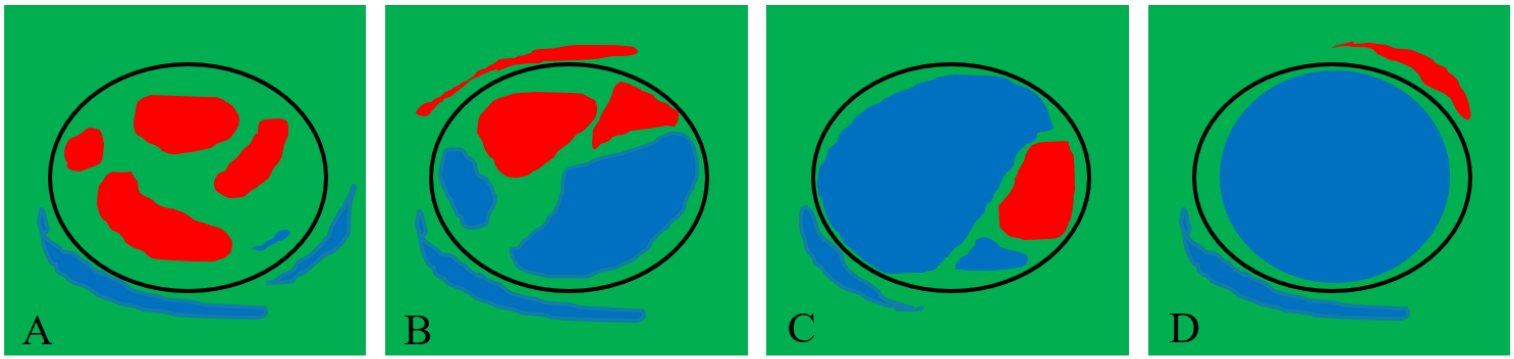

Figure 1. Elastographic pattern used to assess lymph nodes. (A) grade 1, predominantly red and green areas and rarely, blue areas; (B) grade 2, predominantly red and green areas with blue area comprising < 50%; (C) grade 3, predominantly green and blue areas with blue areas comprising > 50%; (D) grade 4, predominantly blue area comprising nearly 100% (lymph node outlined with a dotted line)

3-2-2. Semi-quantitative analysis

For semi-quantitative analyses were performed for the mean hue histogram values and stiffness area ratios in the acquired images. The mean hue histogram (Moon *et al*., 2010) and stiffness area ratios (Nakajima *et al*., 2015) were assessed off-line using Image J® software (National Institutes of Health, Bethesda, MD., USA). The mean hue histogram (Figure 2) (Moon *et al*., 2010) was constructed using the mean pixel color values within the lymph node via the plug-in for hue histogram analysis. First, the color-coded images were obtained by subtracting grey scale images from the original elastographic images to eliminate B-mode information. Second, ROIs were drawn manually around the entire lymph node in B-mode images. These ROIs were superimposed onto the color-coded images and the hue histograms were constructed and after mean values calculated (Preucil, 1953). Values range from 0 to 255 (from red to green to blue), and the increasing stiffness resulted in an increased mean hue histogram value.

Stiffness area ratios (Figure 3) were determined using the following image processing steps. First, ROIs were manually selected to include the lymph node. Second, the stiffer tissue was visualized as a colored pixel determined to be within a certain threshold level (hue: 145-180, brightness: 0-255) (Nakajima et al., 2015). The stiff tissue areas were indicated with red pixels, and the percentage of the stiff tissue area within the ROI was calculated.

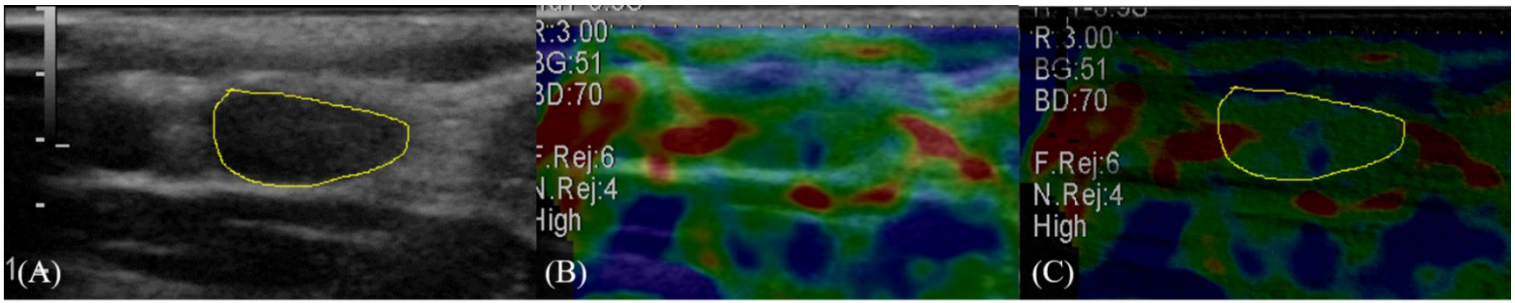

Figure 2. Evaluated mean hue histogram. From original images (A, B), a subtracted (B-A) color-code image (C) with region of interest around the lymph node was obtained and the mean hue histogram was analyzed as used bottom calculation formula.

$$\tan(\boldsymbol{mean\ Hue\ value}) = \frac{\sqrt{\boldsymbol{3}}\,(\boldsymbol{G}-\boldsymbol{B})}{\boldsymbol{2}(\boldsymbol{R}-\boldsymbol{G}-\boldsymbol{B})}$$

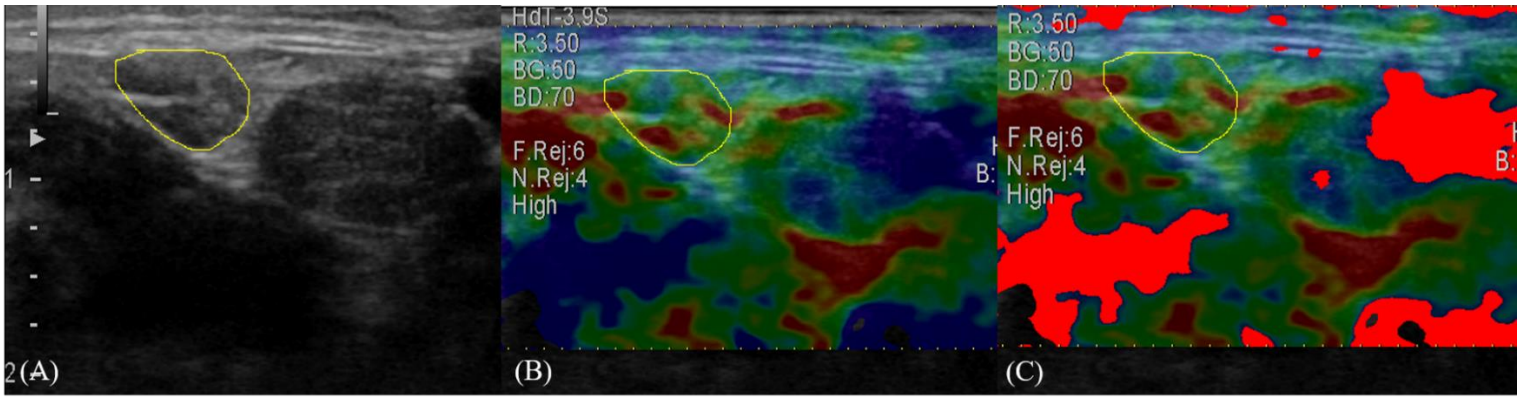

Figure 3. Calculated stiffness area ratios. From a binary image (A, B), the lymph node area was manually selected as the region of interest (C) and the stiffer tissue visualized as a red pixel was determined within a certain threshold level (hue: 145-180, brightness: 0-255).

4. Statistical Analysis

Statistical analysis was performed using SPSS software (IBM SPSS Statistics 22, IBM Corporation, Armonk, NY, USA). Normal distribution of quantitative variables was determined using the Kolmogorov-Smirnov test. Normally distributed data were presented as the mean ± standard deviation (SD), and non-normalized distributed data were presented as the median (range). Normal ranges of elastographic patterns, mean hue histograms and stiffness area ratios were calculated using the fifth and 95th percentiles of the observed data (mean ± 1.96 × SD). Pearson correlation was used to determine the association between age and semi-quantitative strain elastography indices.

The assessment of inter- and intra-observer agreement in the qualitative data analyses was performed using Kappa statistics and quantitative data were analyzed using intra-class correlations (ICC). The strength of agreement was classified based on the following *k* values: poor (*k*: < 0.04), moderate (0.41-0.6), good (0.61-0.79), and excellent (> 0.8) (Viera *et al*, 2005). A *p* value of < 0.05 was considered statistically significant.

RESULTS

1. Animals

Forty-five dogs were evaluated for enrollment in the study. The details of the clinically healthy dogs were as follows: median age was three years (range: 1-12 years) and median body weight was 6.26 kg (range: 2.78-10.25 kg). There were eight females, 11 spayed females, three males and 23 castrated males. The included breeds were Beagle (*n*=1), Cavalier King Charles spaniel (*n*=1), Chihuahua (*n*=3), Coton de tulear (*n*=1), Dachshund (*n*=3), Maltese (*n*=9), miniature Schnauzer (*n*=1), mixed (*n*=5), Pomeranian (*n*=2), Shih-Tzu (*n*=3), Spitz (*n*=10) and toy Poodle (*n*=6).

2. Gray scale ultrasonography

The mandibular lymph node was successfully identified in all dogs. The gray-scale ultrasonographic findings are summarized in Table 1. Mean ± standard deviation (SD) of the left mandibular lymph node's length and width were 0.97 ± 0.37 *cm* and 0.23 ± 0.10 *cm*, respectively. The mean ± SD length-to-width ratio was 0.40 ± 0.10. All mandibular lymph nodes showed an oval shape and smooth margin. The mandibular lymph node was predominantly hypoechoic (95.5%, *n*=43/45 lymph nodes) to isoechoic (4.5%, *n*=2/45 lymph nodes) compared to the adjacent fat.

Table 1. Gray-scale ultrasonographic characteristics of mandibular lymph node in 45 clinically healthy dogs.

Variables	Clinical healthy dogs (*n*=45)
Measurement (mean ± SD)	
Length (cm)	0.97 ± 0.37
Width (cm)	0.23 ± 0.10
Length to width ratio	0.40 ± 0.10
Characteristics (number of dogs)	
Shape	Oval (*n*=45)
Echogenicity	Hypoechoic (*n*=43)
	Isoechoic (*n*=2)
Margin	Smooth (*n*=45)

3. Strain elastography

Clinically healthy mandibular lymph nodes predominantly exhibited homogenous red and green coloration. After elastographic pattern evaluation, all lymph nodes were graded 1 or 2. The cortex and medulla could not be differentiated by strain elastography. The mean hue histogram value was 80.96 ± 8.29 (lower limit: 64.71, upper limit: 97.21). The stiffness area ratio was 0.03 ± 0.02 (lower limit: 0.07, upper limit: 0.01). The elastographic pattern was 1.23 ± 0.42 (lower limit: 2.06, upper limit: 0.40). The mean hue histogram, stiffness area ratio, and elastographic pattern exhibited no correlation with age (Figure 4, Figure 5 and Table 2). Kappa values for elastographic patterns had an inter and intra-observer variability of 0.51 (0.49-0.53), and 0.89 (0.88-0.91), respectively, indicating moderate reproducibility and excellent repeatability. The ICC between observers was 0.86 (0.73-0.92) for the mean hue histogram and 0.88 (0.78-0.93) for stiffness area ratios, indicating excellent inter-observer reproducibility. Furthermore, the ICC for each observer was 0.91 (0.83-0.96) for the mean hue histogram and 0.99 (0.98-0.99) for stiffness area ratios, indicating excellent intra-observer repeatability.

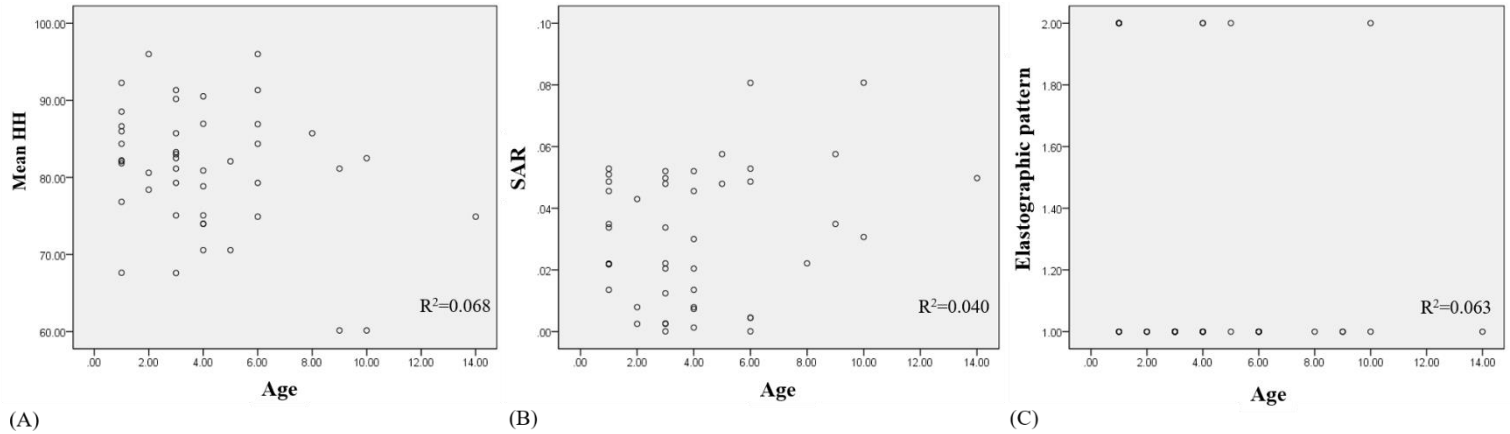

Figure 4. Scatter plots illustrating showed no significant (all $p > 0.05$) correlations (r) between age and the three strain elastographic indices (mean HH (A), SAR (B) and elastographic pattern (C)).

Table 2. Results of correlation from three strain elastographic indices in 45 clinically healthy dogs.

Variable	Age		
	r	R^2	*p* value
Mean hue histogram	-0.261	0.068	0.087
Stiffness area ratio	0.199	0.040	0.196
Elastographic pattern	-0.251	0.063	0.1

DISCUSSION

There were no previous qualitative and semi-quantitative analyses for clinically healthy mandibular lymph nodes. The values showed no correlation with age and moderate to excellent repeatability and reproducibility. Therefore, semi-quantitative strain elastography analysis could be applied to patients with head/neck cancer effectively.

In human medicine, a strain ratio of > 1.5 was most useful for metastatic lymph node classification using ultrasound elastography (Lyshchik *et al*., 2007). However, the experiment did not evaluate strain ratios because only a fixed ROI box could be used in the device. In addition, the mandibular lymph nodes were often too small, or exhibited a heterogeneous pattern, which made it difficult to select where to position the ROI. However, by using Image J for semi-quantitative analysis, it was possible to utilize freely drawn ROIs that could cover the entire lymph node. In addition, a previous report showed that the mean hue histogram values were found to be equal in strain ratio for diagnostic performance (Carlsen *et al*., 2017), and thus, the experiment evaluated only the mean hue histograms.

In human medicine, strain elastography has revealed that the cortex of the lymph node is harder than the hilum and medulla (Carlsen *et al*., 2017; Chiorean *et al*., 2016). Inflammatory lymph nodes have an elastographic appearance similar to that of a normal lymph node, but with a stiffer cortex and a softer hilum (Wojcinski *et al.*, 2012). The cortex of malignant lymph nodes are harder than the cortex of normal lymph nodes and are typically harder than the medulla (Wojcinski *et al*.,

2012), because metastatic cancer cells invade the lymph nodes through afferent lymphatic vessels, with the metastatic focus being initially formed in the peripheral region, remote from the hilum of the lymph nodes (Langenbach *et al*., 2001). In the present study, however, there were no differences between the cortex and the medulla in clinically healthy dogs. The reason for this may be that the lymph nodes were too small to allow differentiation of their anatomic structure. Thus, shear-wave elastographic examination may be needed to accurately analyze the cortex and medulla of these lymph nodes.

Strain elastography for measuring tissue deformity and stiffness is performed after applying external compression. Therefore, the success of this technique is dependent on the operator. Pre-compression should be minimal, with the transducer held lightly in contact with the skin and plenty of gel applied (Barr and Zhang, 2012). Small amplitude movements (heel-toe movement) are all required to induce the required strain of 0.1-2% in the tissue (Dietrich *et al*., 2017). The strain graph was used as a tool for maintaining stable compression in this study. This graph shows the average strain of tissues under compression and the operators can check the appropriate amount of stress being applied in real-time feedback based on the graph. Displacement that is both too large and too small will lead to a poor strain graph. However, the strain graph has no absolute criteria for the selection of appropriate elastographic images. Thus, in order to acquire of the appropriate image, elastographic images were selected when uniform compression was maintained at the lymph node based on the appearance of uniform color. Nevertheless, the

elastographic pattern, mean hue histogram values and stiffness area ratio showed moderate to excellent interobserver reproducibility and excellent intraobserver repeatability. The reason for the inclusion of only the mandibular lymph nodes was that obtaining reproducible elastograms for retropharyngeal lymph nodes difficult, owing to the presence of large vessels and their deep location. This was different compared to other studies (Seiler and Griffith, 2017).

One limitation of the present study is that clinically healthy dogs were selected based on clinical examination (physical examination, blood analysis, and imaging studies) to avoid invasive procedures, such as FNA or biopsy. Thus, it could not elucidate the homogeneity of the clinically healthy group.

Despite the limitations of this study, it showed that semi-quantitative and qualitative strain elastography can provide reliable information regarding the characteristics of clinically healthy mandibular lymph nodes, which may be helpful in evaluating patients with head/neck cancer lymph nodes.

CONCLUSION

Strain elastography is noninvasive, simple, and easy to perform. The study's results indicate that semi-quantitative and qualitative strain elastography can provide reliable information regarding the characteristics of clinically healthy mandibular lymph nodes. The values showed no correlation with age and exhibited moderate to excellent repeatability and reproducibility. Therefore, strain elastography is a useful method for the assessment of mandibular lymph nodes in dogs.

CHAPTER II

Feasibility of lymphosonography for evaluating mandibular lymph nodes in clinically healthy dogs

INTRODUCTION

The sentinel lymph node is defined as the first-draining lymph node and its evaluation is indicated to detect the presence of locoregional nodal metastasis (Tuohy *et al*., 2009; Beer *et al*., 2018). If the sentinel lymph node is normal, further draining lymph nodes are assumed to be normal (no metastasis) and neither sampling nor removal is required (Tuohy *et al*., 2009; Beer *et a*l., 2018). Several techniques have been described for sentinel lymph node detection in veterinary medicine including lymphoscintigraphy, near-infrared fluorescence imaging (NIR) and methylene blue staining (Tuohy *et a*l., 2009; Beer *et al*., 2018; Favril *et al*., 2019), but they have some limitations. Methylene blue dye not only stains the sentinel lymph node but also the adjacent fat, which often obscures the lymph node or leads to a more extensive dissection than necessary (Tuohy *et al*., 2009; Beer *et al*., 2018), and may not provide information on the lymph node status (i.e., reactive or metastatic). NIR is considered a safe and simple technique, but requires a special camera for wavelength detection of 700 to 900 *nm*, with the success of sentinel lymph node visualization depending on the position of the patient, relative to the camera and the distance of the camera to the skin (Favril *et al*., 2019).

Lymphoscintigraphy has several problems. It requires expensive equipment and facilities, involves exposure to radioactive material, and cannot clearly visualize the direct connection between primary sentinel lymph nodes and their afferent lymphatic vessels (Tuohy *et al*., 2009; Beer *et al*., 2018). Computed tomography (CT) lymphography is a complementary technique that requires general anesthesia (Grimes *et al*., 2017; Rossi *et al*., 2018)

Recently, lymphosonography has been utilized to evaluate lymph nodes. Lymphosonography is a new technique for sentinel lymph node biopsy and lymphatic system evaluation that utilizes injection of contrast media to the parenchyma (Goldberg *et al*., 2004). The technique has only been used pre-clinically and tested in proof-of-concept studies mainly involving pigs, dogs, and rabbits usually for evaluating lymph nodes of mammary gland tumors (Goldberg *et al.*, 2005; Lurie *et al*., 2006; Curry *et al*., 2007; Gelb *et al.,* 2010; Goldberg *et al.,* 2011; Liu *et al*., 2014; Favril *et al*., 2019). However, the clinical usefulness of lymphosonography has not yet been demonstrated in dogs. Also, only perflutren lipid microsphere (Definity®) or sulphur hexafluoride microbubbles (Sonovue®) were used with no previous study using perflubutane microbubbles (Sonazoid®) for evaluating lymph nodes in dogs.

Therefore, the aims of this study were to determine the clinical efficacy of lymphosonography for detecting sentinel lymph nodes and to evaluate lymphatic systems in the craniocervical region using perflubutane microbubbles in clinically healthy dogs. This research is a continuation of the previous one involving patients

with head/neck cancer for clinical application. The hypothesis was that lymphosonography could be used as a sentinel lymph node imaging method which would show difference in the characteristics of non-metastatic and metastatic lymph nodes.

MATERIALS AND METHODS

1. Animals

Client-owned and laboratory dogs were included in the study (September 2017-March 2018). Client-owned dogs, presented to the Haemaru Referral Animal Hospital, Seoul, Korea for undergoing regular medical health examination. All owners of these dogs were participated voluntarily. All procedures were performed according to the Ethical Principle in Animal Research adopted by Seoul National University. This experiment was approved by Seoul National University Institutional Animal Care and Use Committee (SNU-170912-24). Dogs were classified as clinical healthy based on routine physical examination, complete blood analysis (including complete blood count, biochemical profile and C-reactive protein level), radiologic examination (thoracic radiography and abdominal ultrasound) and the absence of any known malignancy and inflammation/infection.

2. Animal preparation and anesthesia

The animals were fasted for approximately 8 hrs for general anesthesia. The composition of the anesthesia was a combination of medetomidine (0.02 mg/kg; Domitor, Orion Pharma) and zolazepam/ tiletamine (5 mg/kg; Zoletil 50, Virbac Laboratories), administered via intramuscular injection. Heart rate and respiratory rate were monitored. (Perianesthetic period: 0, 5, and 10 min and recovery phase)

3. Ultrasound procedure

Ultrasonographic examination were performed by the first author using a 2- to 12-MHz linear probe (Arietta 60, Hitachi-aloka, Tokyo, Japan) or a 5-to 12-MHz linear probe (Alpha 7, Aloka, Tokyo, Japan) with adjustments for imaging parameters such as system gain and depth of field. The lymph node (mandibular, medial retropharyngeal) was examined via gray-scale ultrasound and then by lymphosonography was performed.

When performing lymphosonography, a single focal zone was placed at the deepest part of the lesion and the mechanical index was set to minimize microbubble destruction, and gain settings were such that small vessel flow produced a barely detectable color response on pre-contrast images. The mechanical index and B-mode gain were set at 0.22 and 65 dB, respectively. Before the procedure, the contrast agent was reconstituted according to the manufacturer's guidelines. Immediately before injection, the solution was rehomogenized by gently tilting the vial. In clinical healthy dogs, the entire 1 *ml* of the perflubutane microbubble (Sonazoid®, GE Healthcare, Oslo, Norway) was injected at the buccal membrane using a 23-gauge needle. The same person injected all dogs. Any adverse effects associated with contrast media injection were recorded. Once contrast agent was identified at the injection site, the site was gently massaged for up to 1 minute in an attempt to accelerate the movement of the contrast agent into the lymphatic vessel that drained into the mandibular lymph node (Macdonald *et al*., 2008). A video clip was acquired for the first 2 min (13 frames/s); thereafter, images were captured intermittently at 3,

5, 7, and 10 min after injection. If no contrast enhancement was seen, stopped scanning after 10 minutes. Color Doppler examination was used after lymphosonography to confirm the presence of microbubbles and distinguish them from other echogenic structures. This examination might cause the microbubble to rupture, resulting in a characteristic mosaic pattern, which has been referred to as the acoustic emission effect (Blomley *et al.,* 1999).

All images were recorded as a video clip or as images and sent to a PACS (INFINITT, Infinitt Healthcare Co., Ltd., Seoul, South Korea) for off-line analysis.

4. Image analysis

4-1. Quantitative analysis

For quantitative analysis, lymphatic vessels/ mandibular lymph nodes were measured, as well as lymphatic vessel size, contrast agent transit time, and contrast enhancement intensity. Lymph node visualization was defined as positive for microbubble uptake based on a mosaic pattern in the color Doppler examination (Blomley *et al*., 1999). Lymphatic vessels were determined by the short-axis diameter. The contrast transit time was defined as the time taken to initially the lymphatic vessels and mandibular lymph nodes. Contrast enhancement intensity was evaluated using Image J software (Image J®, National Institute of Mental Health, Wayne, USA). Pixel count was measured using the same sized region of interest (ROI) in the mandibular lymph node on pre- and post-contrast images. Values varied from 0 (black) to 255 (white), with a higher value indicating that full contrast enhancement. Measurements of mean, maximum, and standard deviation were obtained for contrast enhancement values.

4-2. Qualitative analysis

The qualitative criteria of contrast enhancement patterns (Figure 5) of lymph nodes were classified into normal or filling defects. Normal was sub-classified into completely filled or capsular enhancement, while filling defect were subclassified into partial or complete filling defects (Server *et al*, 2012).

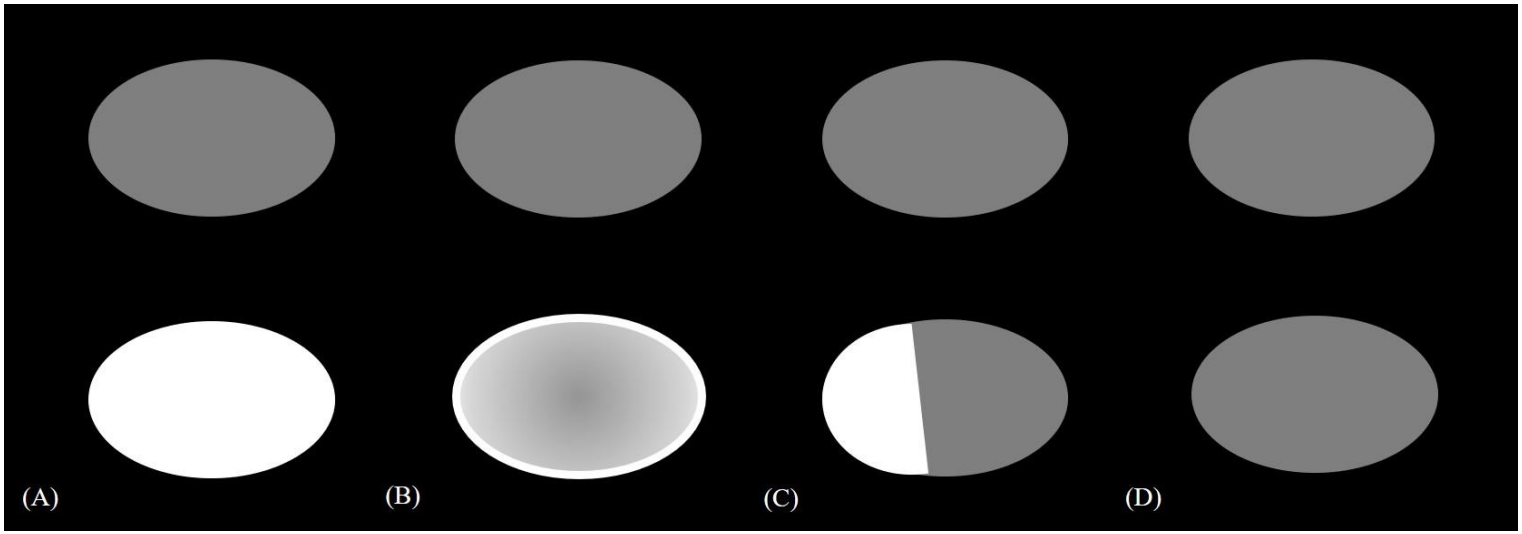

Figure 5. Contrast enhancement pattern of lymph node. Upper panel showed pre-contrast and lower panel showed post-contrast enhancement image. The contrast enhancement pattern was classified as completely filled (A), capsular enhancement (B), partial filling defect (C) or complete filling defect (D).

5. Statistical analysis

Statistical analysis was performed using SPSS software (IBM SPSS Statistics 22, IBM Corporation, Armonk, NY, USA). Contrast enhancement pattern was evaluated using kappa statistics to assess inter-observer agreement. The strength of agreement was classified based on the following *k* values: poor (*k*: < 0.04), moderate (0.41-0.6), good (0.61-0.79), and excellent (> 0.8) (Viera *et al*, 2005). A *p* value of < 0.05 was considered statistically significant.

RESULTS

1. Animals

Eleven clinically healthy dogs were evaluated for enrollment in the study. The characteristics of the clinically healthy group were as follows: median age three years (range: 6 months-12 years); one female, one spayed female, five males and four castrated males; breeds included Beagle (n=5), Dachshund (*n*=2), Miniature Schnauzer (*n*=1), mixed (*n*=1), Pomeranian (*n*=1) and toy poodle (*n*=1) and median body weight was 5 kg (range: 3.18-7.84).

2. Monitoring of anesthesia

Peri-anesthetic heart rates (median, range) were 80 for 0 min (80-150), 70 for 5 min (60-100) and 50 for 10 min (50-70), respectively. Peri-anesthetic respiratory rate (median, range) were 5 for 0 min (4-12), 4 for 5 min (3-4) and 4 for 10 min (3-8), respectively. Recovery (median, range) heart rate was 100 (100-120) and respiratory rate was 8 (5-12).

3. Lymphosonography

All dogs were anesthetized successfully and were able to recover satisfactorily. Before contrast agent administration, mandibular and medial retropharyngeal lymph nodes could be identified by grey-scale ultrasonography as an oval, hypoechoic structure. The full contrast was successfully injected in all cases, and no adverse events were noted. After lymphosonography, only the ipsilateral injection site of the mandibular lymph node was identified.

Because the contrast agent traveled very superficially in the afferent lymphatic vessels, a non-compression scan technique was necessary. Additionally, if the enhanced lymph node was first found, scanning was performed to detect its corresponding lymphatic vessels by tracing back from the node.

The lymphosonographic findings are summarized in Table 3.

Table 3. Lymphosonographic findings in clinically healthy mandibular lymph nodes

Variables			Clinically healthy (*n*=11)
Quantitative analysis	Visualization [a]	Lymphatic vessels	8
		Lymph node	11
	Lymphatic vessels diameter (*mm*) [b]		1.2 (0.7-1.8)
	Contrast transit time (min) [b]	Lymphatic vessel	5 (5-7)
		Lymph node	5 (1-7)
	Lymph node enhancement mean intensity [b]		64.53 (24.81-128.43)
Qualitative analysis	Lymph node enhancement pattern [a]	Completely filled	6
		Capsular filling	5
		Focal filling defect	0
		Full filling defect	0

[a] Data area expressed as number of dogs. [b] Data are expressed as median (range).

4. Image analysis

4-1. Quantitative analysis

After mucosal administration of perflubutane microbubbles, enhanced lymphatic vessels (*n*=8/11) and mandibular lymph nodes (*n*=11/11) detected. On lymphosonography, the afferent lymphatic vessels were demonstrated as hyperechoic linear structures leading from the injection site. The measured median (range) was 1.2 (0.7-1.8) *mm* with these vessels readily traced to their mandibular lymph nodes (Figure 6). In addition, the movement of contrast material in the lymphatic vessels was observed in real-time. However, visualization of the efferent lymphatic vessels or the second-echelon lymph was not possible in any dog.

The normal lymphatic vessels were visualized within five min post-injection and the mandibular lymph nodes were identified after simultaneous enhancement with lymphatic vessels that lasted 10 min post-injection. The mean intensity contrast enhancement value was 64.53 (median, range: 24.81-128.43)

4-2. Qualitative analysis

Two enhancement patterns were observed in the mandibular lymph nodes of clinically healthy dogs. In capsular enhancement (*n*=5/11, Figure 7A), the enhanced capsular area extended gradually, but the lymph node parenchyma did not show enhancement. Capsular filling was only identified in dogs aged under 1-year-old (*n*=4/5). In completely filled enhancement (*n*=6/11, Figure 7B), the lymph node capsule was first enhanced and became hyperechoic, while the parenchyma was subsequently enhanced centripetally and homogenously.

Color Doppler imaging is a useful method to differentiate the contrast-enhanced lymph node from other hyperechoic tissues (eg., fibrous tissue). After injection of perflubutane microbubbles, typical acoustic emission mosaic color pattern was observed within the mandibular lymph nodes (Figure 8).

The kappa statistics of contrast enhancement pattern was 0.814, indicating excellent inter-observer agreement

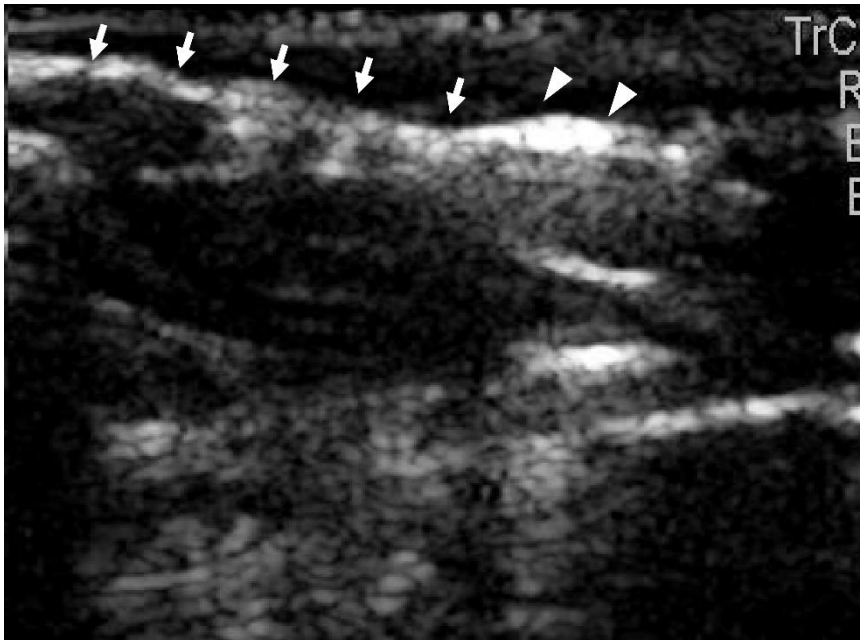

Figure 6. Morphology of lymphatic vessels and lymph node (LN) after lymphosonography in clinically healthy mandibular LN. After contrast media injection in oral buccal mucosa, a hyperechoic lymphatic vessel (arrows) was identified and traced into enhanced LN (arrows head).

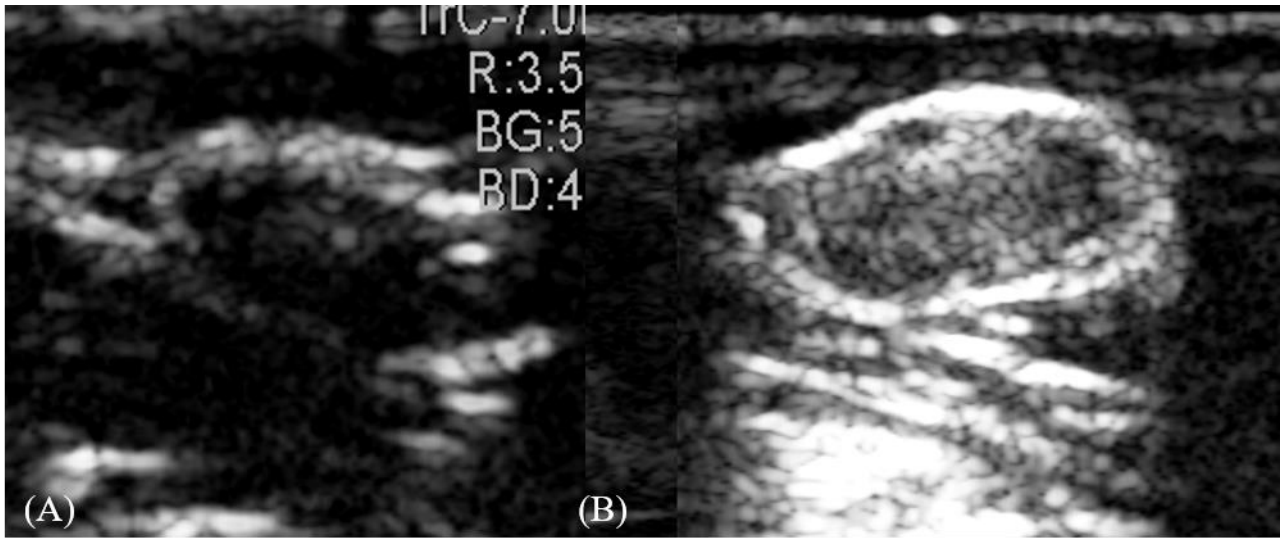

Figure 7. Different types of contrast enhancement pattern of clinically healthy lymph node. The enhancement of the entire capsule giving a capsular enhancement appearance (A) or homogeneous centripetally enhancement with completely filled (B).

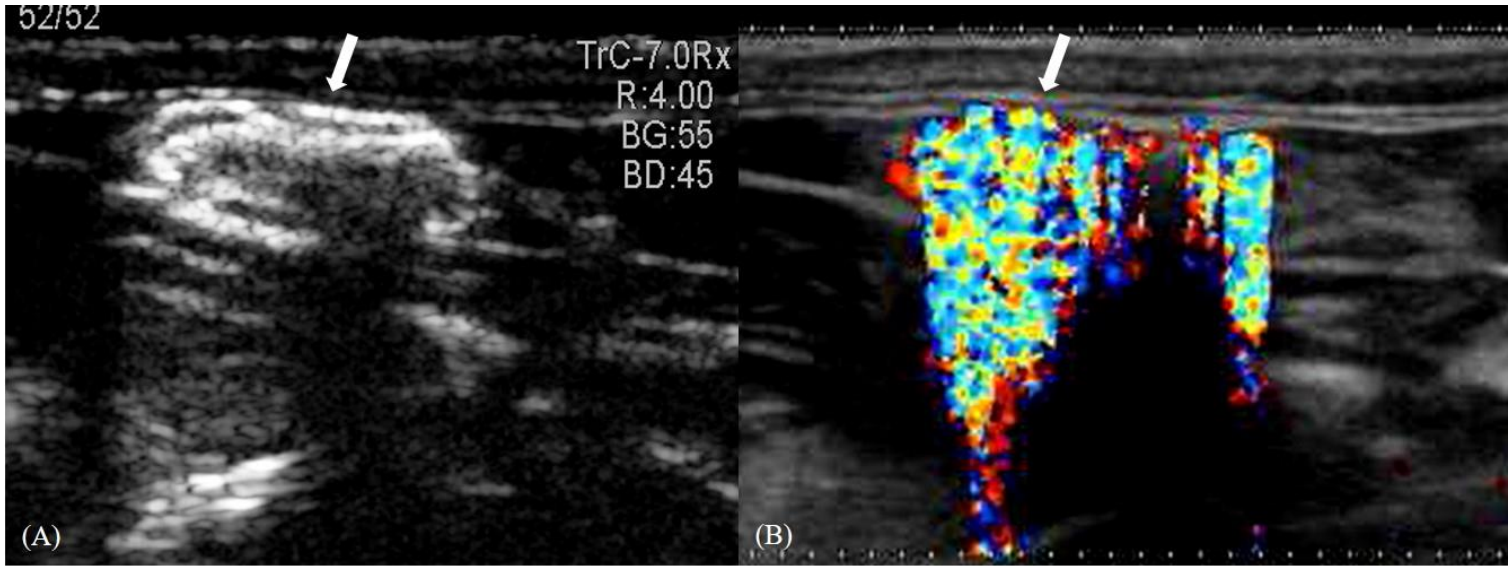

Figure 8. Confirmation of contrast within lymph node (LN) with color Doppler imaging of the acoustic emission (AE) phenomenon. (A) After mucosal injection of perflubutane microbubbles, echogenic structure (arrow) were identified and thought to represent contrast-enhanced LN. (B) When color Doppler imaging was used to evaluate these structures, the AE effect (arrow) was shown confirming that they contained contrast microbubble.

DISCUSSION

Parenchymal injection of perflubutane microbubbles is known to be method for sentinel lymph node localization. However, this experiment showed that lymphosonography was not an adequate sentinel lymph node imaging method for the craniocervical region because of restricted visualization of some lymph nodes (e.g. buccal, parotid and superficial cervical lymph nodes) due to the adjacent bone structure. Furthermore, this study did not conduct a control technique (e.g., methylene blue dye) thus limiting it to the use of the sentinel lymph node finding method. In the experiment, only one dog had multiple mandibular lymph nodes identified prior to contrast agent administration but among them, one lymph node showed contrast enhancement. Thus it was possible to conclusively determined the sentinel lymph node. However, further research is needed.

Instead of finding sentinel lymph nodes, this experiment clearly shows that lymphosonography could be used to detect lymphatic drainage pathways. The one-milliliter contrast agent dose allowed good visualization leading up to and filling the lymph node. In the lymph node, lymphatic fluid drains from the afferent lymphatic vessel into the subcapsular sinus, which is connected to the medullary sinus through a complex trabecular sinus network and exist through the efferent vessels (Ikomi *et al.,* 2012). In this study, when the perflubutane microbubbles arrive via the afferent lymphatics to the lymph nodes, the subcapsular sinus enhancement was appreciated. This ranged from capsular filling to complete filling. Capsular filling enhancement was observed only in young dogs (under 1-year-old) possibly due to their

physiological status (i.e., extramedullary hematopoiesis), but additional histological confirmation is needed.

The time after contrast agent injection to its visualization (contrast transit time) in the mandibular lymph node varied in clinically healthy dogs. The median time after injection of contrast agent to visualization within the lymphatic vessels and mandibular lymph node was 5 min for both. which was similar to the results of previous reports using inhalation anesthesia (Nielsen *et al.* 2008). It has been showed that different anesthetic methods do not affect lymphatic system visualization. Furthermore, when metastases start in the lymph node, tumor cells arrive by afferent lymphatic ducts in the subcapsular sinus and peripheral neoangiogenesis begins. Tumoral infiltration then progresses to the medullary sinus and the perinodal fat and changed lymphatic flow (Sinem and Michael, 2014). Because the contrast transit time reflected lymphatic flow of clinically healthy lymph nodes and lymphosonographic findings of clinically healthy dogs were compared with those of cancer patients, it was possible to provide predictive information regarding metastasis.

A previous study using non-intravenous administration of sonographic contrast agents for lymphatic visualization had been performed (Favril *et al.,* 2019). However, the study did not use a mononuclear phagocyte specific (previously, reticulo-endothelial system, RES) uptake agent. Compared with sulfur hexafluoride microbubbles (Sonovue®, non RES-specific agent), perflubutane microbubbles (Sonazoid®, RES-specific agent) can fill the lymph node better because the agent

remains intact after being phagocytosed by normal lymph node macrophages (Gold berg *et al.,* 2004; Gold berg *et al.,* 2005; Gold berg *et al.,* 2011; Matsuzawa *et al*., 2015). Furthermore, perflubutane microbubbles (Sonazoid®) have other advantages for determining hepatic parenchymal metastasis (Kanemoto *et al*., 2009; Nakamura *et al*., 2010). Therefore, this contrast agent was selected for the present study.

In previous reports (Goldberg *et al*., 2005), intravenous administration of perflubutane microbubbles (Sonazoid®), did not result in prolonged lymph node enhancement, indicating a lack of lymph nodes uptake. This is likely related to the fact that macrophages line the lymphatic vessels within the lymph node and not the intranodal blood vessels. Therefore, for detecting lymph nodes, another injection route such as lymphosonography is recommended. In addition, scanning electron microscopy confirmed that perflubutane microbubbles are removed by normal macrophages in the first-draining lymph node (Goldberg *et al*., 2011). For visualization of second-echelon lymph nodes, injection of contrast media into the first- draining lymph nodes is recommended (Liu *et al*., 2014).

One limitation of the present study is that clinically healthy dogs were selected based on clinical examination (physical examination, blood analysis and imaging studies) to avoid invasive procedures, such as FNA or biopsy. In addition, no control technique was performed (e.g. methylene blue dye or lymphoscintigraphy) and for the evaluation of the lymph nodes using the sentinel lymph node imaging method.

In conclusion, although lymphosonography showed limited use finding sentinel lymph nodes in the craniocervical region, this method was able to clearly

show lymphatic drainage pathways (lymphatic vessels and lymph nodes). Additional research is necessary to determine the clinical application of this new method for cancer patients.

CONCLUSION

Lymphosonography using perflubutane microbubbles is easily performed and can directly visualize the lymphatic vessels/mandibular lymph nodes. Contrast enhancement within lymph nodes/ lymphatic vessels was identified approximately five min post-injection. Two enhancement patterns were observed in the lymph nodes of clinically healthy dogs. In complete filling, the lymph node capsule was first enhanced and became hyperechoic, while the parenchyma was subsequently enhanced centripetally and homogenously. In capsular enhancement, the enhanced capsular area extended gradually, but the lymph node parenchyma did not show enhancement. This pattern was identified only in young dogs (under 1-year-old). Based on these results, lymphosonography could be used to evaluate lymph nodes for comparison with cancer patients.

CHAPTER III

Evaluating mandibular lymph node malignancy in normal and head/neck cancer dogs using contrast-enhanced ultrasound sonography combined with strain elastography

INTRODUCTION

Determining lymph node metastases in dogs with neoplasia is important in staging and developing a therapeutic plan (Herring *et al*., 2002). Several studies have attempted to diagnose metastatic lymph nodes, but the results are often controversial (Nyman *et al*., 2006; Nyman and O'Brien, 2007; Seiler and Griffith, 2018; Belotta *et al*., 2019).

Recently, lymphosonography and ultrasound elastography have been utilized to evaluate lymph nodes. Lymphosonography is a new technique for sentinel lymph node visualization and lymphatic system evaluation that utilizes parenchymal injection of contrast media (Goldberg *et al*., 2004). This technique supplements cytology/biopsy procedures through visualization of the lymphatic system (Goldberg *et al*., 2004; Lurie *et al*., 2006; Favril *et al*., 2019) or is used as one of method for detecting sentinel lymph nodes. Elastography is an imaging modality used to map the elastic properties of soft tissues (Bhatia *et al*., 2010). Malignant tissues tend to be stiffer than normal tissues as they contain an increased density of tumor cells, vasculature, and fibrotic material (Tan *et al*., 2010; Thomas *et al*., 2006; Burnside *et*

al., 2007; Regner *et al.,* 2006). Given these properties, elastography has been used to assess various human organs for malignancy (Tan *et al*., 2010; Thomas *et al*., 2006; Burnside *et al*., 2007; Regner *et al*., 2006; Desmots *et al*., 2016; Alam *et al*., 2008). The successful use of strain elastography for qualitative analysis of lymph nodes has also been reported in veterinary medicine (Seiler and Griffith, 2018; Belotta *et al*., 2019). However, the use of lymphosonography and/or strain elastography for evaluating head/neck cancer in dogs has not yet been explored.

Therefore, the present study aimed to evaluate the diagnostic performance and determine cutoff values for predicting mandibular lymph node malignancy using qualitative and semi-quantitative strain elastography. Furthermore, lymphosonography, evaluated the mandibular lymph nodes and compared clinically healthy dogs to patients with head and neck cancer. The hypothesis was that clinically healthy, non-metastatic and metastatic lymph nodes would show different findings upon lymphosonography and strain elastography, which could improve the diagnostic accuracy for predicting lymph node metastasis.

MATERIALS AND METHODS

1. Animals

1-1. Clinically healthy group

For strain elastography, forty-five dogs were evaluated for enrollment in the study. The details of the clinically healthy group was as follows: median age of 3 years (range: 1-12 years); eight females, 11 spayed females, three males and 23 castrated males; and the included breeds were Beagle (*n*=1), Maltese (*n*=9), toy Poodle (*n*=6), mixed (*n*=5), Chihuahua (*n*= 3), Dachshund (*n*=3), Shih-Tzu (*n*=3), Pomeranian (*n*=2), Cavalier King Charles spaniel (*n*=1), Coton de tulear (*n*=1), miniature Schnauzer (*n*=1) and Spitz (*n*=10). For lymphosonography, eleven clinically healthy dogs were evaluated for enrollment in the study. The clinically healthy group was as follows: median age 3 years (range: 6 months-12 years); one female, one spayed female, five males and four castrated males; breeds included Pomeranian (*n*=1), Dachshund (*n*=2), toy poodle (*n*=1), Miniature Schnauzer (*n*=1), Beagle (*n*=5), and mixed (*n*=1).

1-2. Patients those with head/neck cancer group

Client-owned dogs, presented to the Haemaru Referral Animal Hospital, Seoul, Korea were included in the study (September 2017-December 2018). The visiting purpose of these dogs was evaluating head/neck cancer. All of owners of these dogs were participated voluntarily. All procedures were performed according to the Ethical Principle in Animal Research adopted by Seoul National University. This experiment was approved by Seoul National University Institutional Animal Care and Use Committee (SNU-170912-24). The dogs that got owners' agreement at additional period were enrolled. The included dogs whose owners agreed to allow cytological or histopathological confirmation of mandibular lymph nodes and primary head and/or neck cancer. Lymph nodes with non-diagnostic cytology results (low cellularity or unclear diagnosis) were excluded. Cytological results from normal lymph nodes showed small lymphocytes (75-95%); reactive nodes showed intermediate/ large lymphocytes (15-25%); and metastatic nodes showed cells in the primary tumor site (Cowell *et al*., 2003).

For strain elastography, twelve dogs were evaluated for enrollment in the study. One patient was excluded because of non-diagnostic cytology results. The details of the patient group was as follows: median age of 13 years (range: 2-14 years); three females, five spayed females, one male, and two castrated males; and the included breeds were Maltese (*n*=5), English Cocker spaniel (*n*=2), Borzoi (*n*=1), miniature Schnauzer (*n*=1), Scottish terrier (*n*=1), and Pomeranian (*n*=1). Among the patients, 21 ipsilateral mandibular lymph nodes were evaluated. According to cytology (*n*=19)

or histopathology (*n*=2), lymph nodes were categorized as metastatic (*n*=13) or non-metastatic (*n*=8) status. The primary cancer sites included the following: the oral cavity (squamous cell carcinoma, n=2; inflammation, n=1; melanoma, n=2; epulis, n=1; giant cell granuloma, n=1), the nasal cavity and retrobulbar region (adenocarcinoma, n=1), tonsils (squamous cell carcinoma, n=1) and the cervical region (melanoma, n=1; lipoma, n=1). For lymphosonography, eleven dogs were evaluated for enrollment in the study. The details of the patient group was as follows: median age of 12 years (range: 13-14 years); three females, six spayed females, one male, and one castrated males; and the included breeds were Maltese (*n*=6), English Cocker spaniel (*n*=2), Borzoi (*n*=1), miniature Schnauzer (*n*=1) and Scottish terrier (*n*=1). According to cytology (*n*=9) or histopathology (*n*=2), lymph nodes were categorized as metastatic (*n*=6) or non-metastatic (*n*=5) status. The primary cancer sites included the following: the oral cavity (squamous cell carcinoma, n=2; inflammation, n=1; melanoma, n=3; epulis, n=1; giant cell granuloma, n=1), the nasal cavity and retrobulbar region (adenocarcinoma, n=1) and the cervical region (melanoma, n=1; lipoma, n=1).

2. Ultrasound procedure

B-mode ultrasonography (Arietta V60 or Aloka Prosound Alpha 7), strain elastography (Arietta V60), and lymphosonography (Arietta V60 or Aloka Prosound Alpha 7) were performed. The same device was used for all examination in each dog. The ipsilateral injection site for lymphosonography of mandibular lymph was imaged in the clinically healthy and patient groups. The lymph nodes were examined via grey-scale ultrasound first, and then by strain elastography and/or lymphosonography. During lymphosonography, the dogs were induced anesthesia using a combination drug of medetomidine (0.02 mg/kg; Domitor, Orion Pharma) and zolazepam/ tiletamine (5 mg/kg; Zoletil 50, Virbac Laboratories), administered via intramuscular injection. All images were sent to a PACS (INFINITT, Infinitt Healthcare Co., Ltd., Seoul, South Korea) and were then saved as bit-map files for later analysis.

2-1. Strain elastography

Strain elastography was performed using a 2-12 MHz linear transducer (Arietta 60, Hitachi-aloka, Tokyo, Japan). After acquiring a grey-scale ultrasonography image of the mandibular lymph node in the longitudinal plane, a region of interest comprising the lymph node and surrounding tissue was selected. For strain elastography, compression with light pressure followed by decompression was applied repeatedly until a stable image was obtained. The direction of compression was upwards and then downwards. Real-time elastographic and B-mode images simultaneously appeared side-by-side on the screen. Regions-of-interest (ROIs) included the target lymph nodes, but no other tissues (e.g., bone, blood vessel) that may disturb analysis of the relative stiffness of the target lymph nodes. At least three elastographic images were obtained and these measurements were performed by two investigators independently for analysis of reproducibility. In cases in which acquisition of uniform and regular movements was not feasible, nodes were excluded from the analysis.

All ultrasound elastographic images were displayed using 256-color mapping of each pixel according to the degree of strain with the color scale going from red (highest strain, softest) to, green (average strain, intermediate), to blue (no strain, hardest).

2-2. Lymphosonography

Ultrasonographic examination were performed by the first author using a 2- to 12-MHz linear probe (Arietta 60, Hitachi-aloka, Tokyo, Japan) or a 5-to 12-MHz linear probe (Alpha 7, Aloka, Tokyo, Japan) with adjustments for imaging parameters such as system gain and depth of field.

When performing lymphosonography, a single focal zone was placed at the deepest part of the lesion and the mechanical index was minimize microbubble destruction, and gain settings were such that small vessel flow produced a barely detectable color response on pre-contrast images. The mechanical index and B-mode gain were set at 0.22 and 65 dB, respectively. Before the procedure, the contrast agent was reconstituted according to the manufacturer's guidelines. Immediately before injection, the solution was rehomogenized by gently tilting the vial. One milliliter of perflubutane microbubble (Sonazoid®, GE Healthcare, Oslo, Norway) was injected in the buccal mucosa in clinically healthy dogs or the peritumoral site in dogs with head and neck tumors (Goldberg *et al.,* 2011) using a 23-gauge needle. The same person injected all dogs. Any adverse effects associated with contrast media injection were recorded. Once contrast agent was identified at the injection site, the site was gently massaged for up to 1 minute in an attempt to accelerate the movement of the contrast agent into the lymphatic vessel that drained into the mandibular lymph node (Macdonald *et al.,* 2008). A video clip was acquired for the first 2 min (13 frames/s); thereafter, images were captured intermittently at 3, 5, 7, and 10 min after injection. If no contrast enhancement was seen, we stopped

scanning after 10 minutes. Color Doppler examination was used after lymphosonography to confirm the presence of microbubbles and distinguish them from other echogenic structures. This examination might cause the microbubble to rupture, resulting in a characteristic mosaic pattern, which has been referred to as the acoustic emission effect (Blomley *et al*., 1999).

3. Image analysis

3-1. Grey scale ultrasonography

B-mode images were evaluated on the basis of size, shape of the lymph node, presence of the hyperechoic hilum, margin and echogenicity. The height of the lymph node (in cm) was evaluated to determine size. Length-to-height ratio was used to determine shape. The lymph node margins were classified as irregular or smooth. Lymph node echogenicity was classified as hypoechoic or isoechoic as compared to adjacent fat.

3-2. Strain elastography

3-2-1. Qualitative analysis

The strain elastography was performed three times for each lymph node and the values were averaged for analysis. If the patient had enlargement of multiple lymph nodes, all lymph nodes were analyzed, and the average calculated.

Strain elastographic images were evaluated qualitatively and semi-quantitatively. If an anechoic structure (suspected cystic or necrotic changes) was found in the parenchyma, it was not included in the analysis because these are not indicative of a solid component. In those cases, the remain parenchyma was evaluated. For qualitative analysis, the elastographic patterns were classified based on the distribution and percentage of the lymph node area to the hardness area (blue), subjectively (Figure 9) (Alam *et al*., 2008).

1. Grade 1 indicated absent or very low stiffness (i.e., blue)
2. Grade 2 indicated a stiff area comprising < 50% of the lymph node
3. Grade 3 indicated a stiff area comprising > 50% of the lymph node
4. Grade 4 indicated a lymph node with predominant stiffness that occupied the entire lymph node space

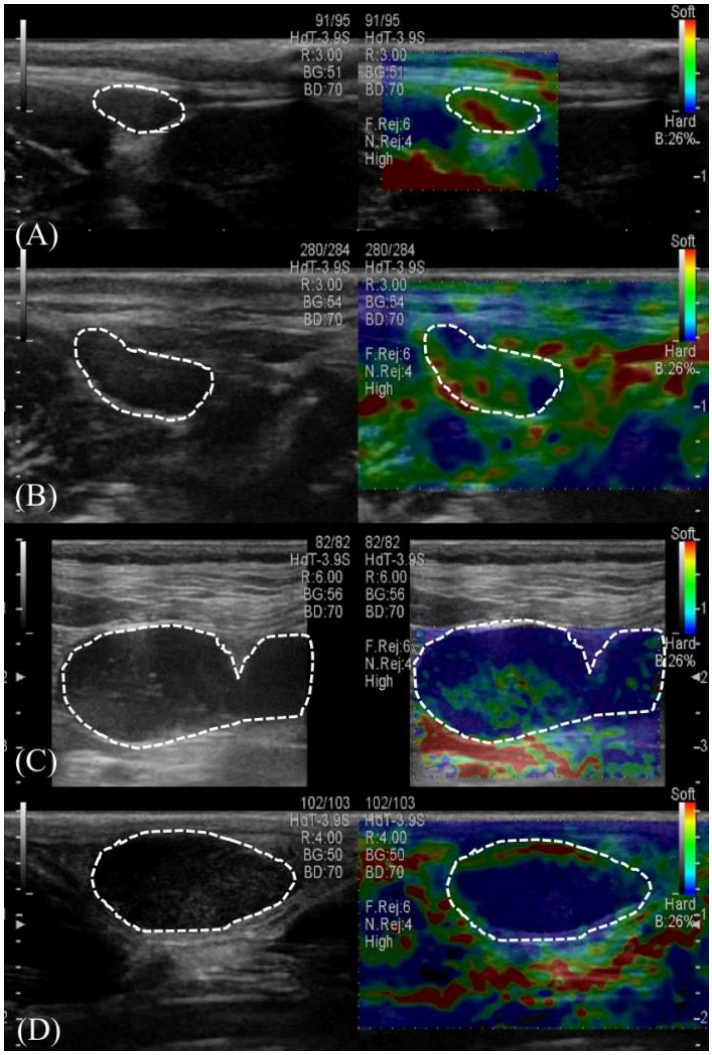

Figure 9. Elastographic pattern used to assess lymph nodes. (A) grade 1, predominantly red and green areas and rarely, blue areas; (B) grade 2, predominantly red and green areas with blue area comprising < 50%; (C) grade 3, predominantly green and blue areas with blue areas comprising > 50%; (D) grade 4, predominantly blue area comprising nearly 100% (lymph node outlined with a dotted line)

3-2-2. Semi-quantitative analysis

For semi-quantitative analyses were performed for the mean hue histogram values and stiffness area ratios in the acquired images. The mean hue histogram (Moon *et al*., 2010) and stiffness area ratios (Nakajima *et al.,* 2015) were assessed off-line using Image J software (National Institutes of Health, Bethesda, MD., USA). The mean hue histogram (Figure 10) (Moon *et al*., 2010) was constructed using the mean pixel color values within the lymph node via the plug-in for hue histogram analysis. First, the color-coded images were obtained by subtracting grey scale images from the original elastographic images to eliminate B-mode information. Second, ROIs were drawn manually around the entire lymph node in B-mode images. These ROIs were superimposed onto the color-coded images and the hue histograms were constructed and after mean values calculated (Preucil, 1953). Values range from 0 to 255 (from red to green to blue), and the increasing stiffness resulted in an increased mean hue histogram value.

Stiffness area ratios (Figure 11) were determined using the following image processing steps. First, ROIs were manually selected to include the lymph node. Second, the stiffer tissue was visualized as a colored pixel determined to be within a certain threshold level (hue: 145-180, brightness: 0-255) (Nakajima *et al*., 2015). The stiff tissue areas were indicated with red pixels, and the percentage of the stiff tissue area within the ROI was calculated.

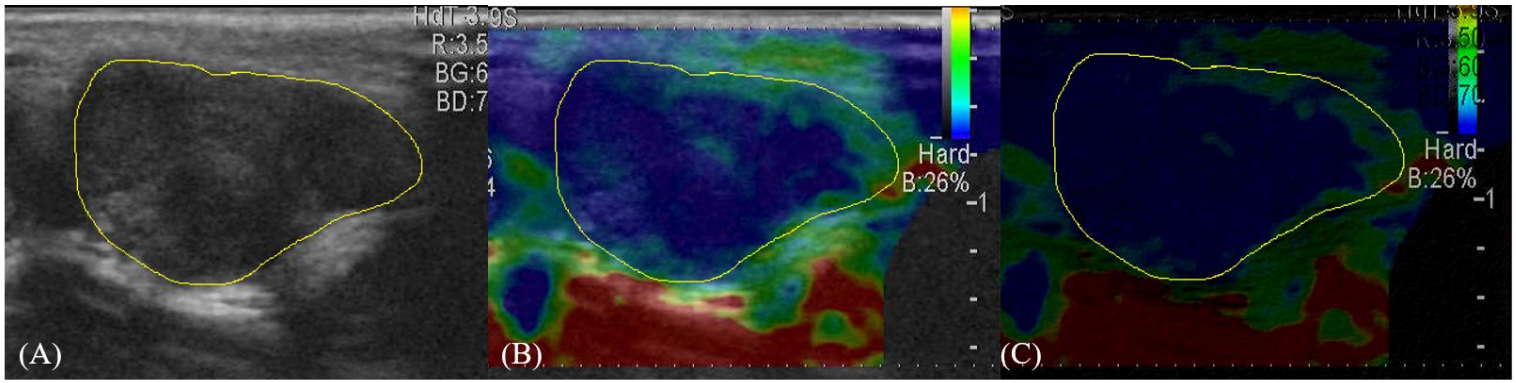

Figure 10. Evaluated mean hue histogram. From original images (A, B), a subtracted (B-A) color-code image (C) with region of interest around the lymph node was obtained and the mean hue histogram was analyzed as used bottom calculation formula.

$$\tan(\boldsymbol{mean\ Hue\ value}) = \frac{\sqrt{\boldsymbol{3}}\ (\boldsymbol{G} - \boldsymbol{B})}{\boldsymbol{2}(\boldsymbol{R} - \boldsymbol{G} - \boldsymbol{B})}$$

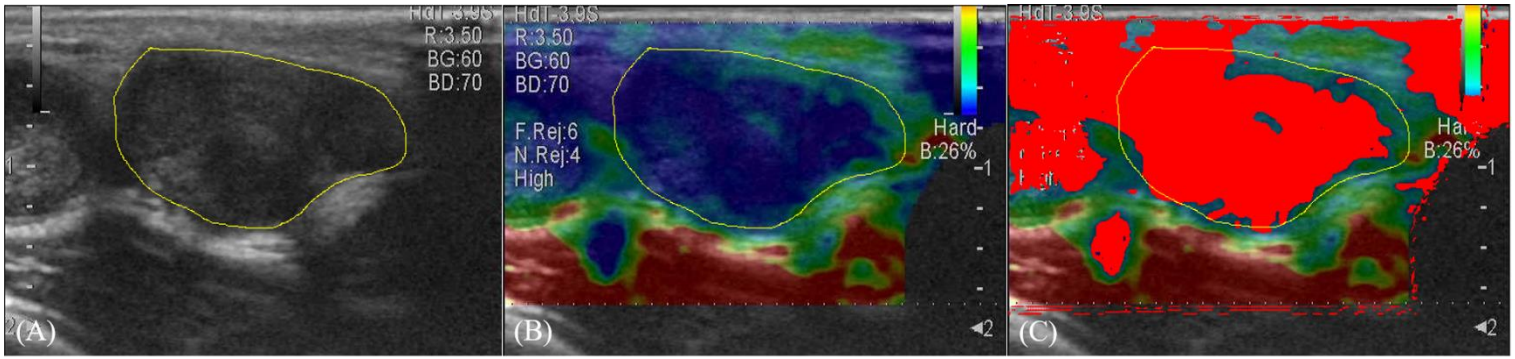

Figure 11. Calculated stiffness area ratios. From a binary image (A, B), the lymph node area was manually selected as the region of interest (C) and the stiffer tissue visualized as a red pixel was determined within a certain threshold level (hue: 145-180, brightness: 0-255).

3-3. Lymphosonography

3-3-1. Quantitative analysis

For quantitative analysis, confirmed the lymphatic vessels/ mandibular lymph nodes and measured lymphatic vessel size, contrast agent transit time and contrast enhancement intensity. The lymph nodes visualization was defined as positive for microbubble uptake based on a mosaic pattern in the color Doppler examination (Blomley *et al*., 1999). The lymphatic vessel sized determined by the short-axis diameter. The contrast transit time defined as first time to visualization of lymphatic vessels and mandibular lymph node. Contrast enhancement intensity was evaluated using Image J software (Image J®, National institute of mental health, Wayne, USA). The pixel count was measured using a same sized region of interest (ROI) in the mandibular lymph node on pre and post contrast images. The values varied from 0 (black) to 255 (white) and higher value meant that fully contrast enhancement. Measurements of mean, maximum, and standard deviation were obtained for contrast enhancement values.

3-3-2. Qualitative analysis

The qualitative criteria of contrast enhancement pattern (Figure 5) were classified as normal or filling defect. Normal was sub-classified as completely filled or capsular enhancement and filling defect was subclassified as partial or complete filling defect (Server *et al*, 2012).

3-4. Strain elastography combined with lymphosonography

The combined score (Alam *et al.*2008) for the mandibular lymph nodes was the sum of the elastographic patterns of strain elastography and contrast enhancement patterns of lymphosonography. Strain elastographic patterns were determined for four criteria: grade 1, 2, 3 and 4 were assigned scores of 2, 4, 6 and 8, respectively. Contrast enhancement patterns on lymphosonography were determined for four criteria: complete filling (score of 2), capsular filling (score of 4), partial filling defect (score of 6) and complete filling defect (score of 8). A statistically supported cutoff line between metastatic and non-metastatic/ clinically healthy lymph nodes was a score of 9.

4. Statistical analysis

After grey-scale ultrasonography, strain elastography and lymphosonography, the results were classified into three groups (clinically healthy, non-metastatic and metastatic lymph nodes) and statistical analyses were performed using SPSS software (IBM SPSS Statistics 22, IBM Corporation, Armonk, NY, USA). Normal distribution of variables was determined using the Kolmogorov-Smirnov test. Normally distributed data were presented as mean ± standard deviation (SD). Non-normally distributed data were presented as medians (range). Quantitative variables for each analysis was compared across groups using a one-way analysis of variance (ANOVA), while qualitative variables for each analysis was compared using the Kruskal-Wallis test. Bonferroni corrected Mann-Whitney tests were performed for post hoc multiple comparisons when significant differences were identified after ANOVA or Kruskal-Wallis test. A p value of < 0.05 was considered statistically significant

4-1. Grey-scale ultrasonography

Quantitative variables, including size and width-to-depth ratio; and qualitative variables, including presence of hyperechoic hilum/ margin and parenchymal echogenicity were compared across groups using statistical analysis.

4-2. Strain elastography

Quantitative variables, including mean hue histogram/ stiffness area ratios and qualitative variables, including elastographic patterns were compared across groups using statistical analysis.

To evaluate the diagnostic performance of the variables that were significantly different between non-metastatic and metastatic lymph nodes, optimal cutoff values were determined using receiver operating characteristic (ROC) curves. All values were determined using the Youden index. Areas under the curve (AUCs) were calculated with 95% confidence intervals (CIs) to quantify the ability of each variable to detect malignancy.

4-3. Lymphosonography

Quantitative variables including lymphatic vessel diameter/ contrast media transit time/ lymph node enhancement intensity and qualitative variables including contrast enhancement pattern were compared across groups using statistical analysis.

4-4. Strain elastography combined with lymphosonography

The combined scores were compared across groups using statistical analysis. To evaluate the diagnostic performance of the variables (e.g., sensitivity and specificity) receiver operating characteristic (ROC) curves were used in the multivariate analysis to determine the different test efficacies. Areas under the curve (AUCs) were calculated with 95% confidence intervals (CIs) to quantify the ability of each variable to predict malignancy.

RESULTS

1. Gray scale ultrasonography

Sonographic findings of lymph node are summarized in Table 4. On grey-scale ultrasonography, there were significant difference ($p < 0.05$) in width-to-depth ratio of > 0.5 for metastatic lymph nodes compared to clinically healthy and non-metastatic lymph node. Otherwise, no statistically significant difference was detected for depth, parenchymal echogenicity, irregular margin, and hyperechoic hilum definition. However, increased lymph node depth and absence of hyperechoic hilum were more frequent in metastatic nodes.

Table 4. B-mode characteristics of the conventional ultrasonography evaluated criteria for the different groups of lymph nodes.

		Clinically healthy (n=45)	Non-metastatic (n=8)	Metastatic (n=13)
Depth (mean ± SD cm)		0.37± 0.11	0.85± 0.65	0.95 ± 0.51
Width-to-depth ratio	< 0.5	39	5	4
	> 0.5	6	0	3 *
Hyperechoic hilum	Present	27	2	1
	Absent	18	3	6
Echogenicity	Normal	45	4	1
	Abnormal	0	1	6
Margin	Smooth	45	5	5
	Irregular	0	0	2

SD, Standard deviation

* indicated significant difference ($p < 0.05$) between clinically healthy and non-metastatic lymph node.

2. Strain elastography

Elastographic findings are summarized in Table 5. Elastographic patterns, mean hue histogram values and stiffness area ratio were significantly different in metastatic lymph nodes compared to non-metastatic and clinically healthy lymph nodes ($p < 0.01$, Figure 11). Clinically healthy and non-metastatic lymph nodes with either grade 1 or 2, reflecting relatively soft elasticity. Metastatic lymph nodes were mostly grade 3 or 4, reflecting relatively stiff elasticity, except for one lymph node.

The diagnostic performance of B-mode and elastography variables are summarized in Table 6. ROC analyses revealed that the best cut-off values for the prediction of metastatic lymph nodes were 92.26 for the mean hue histogram ($p < 0.01$), with a sensitivity of 100% and specificity of 92%, 0.17 for stiffness area ratios ($p < 0.01$), with a sensitivity of 86% and specificity of 100%, and grade 2 for elastographic pattern ($p < 0.01$), with a sensitivity of 86% and specificity of 100%. Among the variables, the mean hue histogram values showed the highest AUC, 0.982 (95% CI, 0.878-1.000) (Figure 12).

Table 5. Qualitative and semi-quantitative analysis of clinical healthy, non-metastatic, and metastatic lymph nodes on strain elastography.

	Clinically healthy (*n*=45)	Non metastatic (*n*=8)	Metastasis (*n*=13)
Elastographic pattern	1.56 ± 0.50	1.50 ± 0.53	3.31 ± 0.85**
Mean hue histogram	81.48 ± 7.86	86.99 ± 4.73	101.35 ± 8.80**
Stiffness area ratio	0.03 ± 0.02	0.05 ± 0.06	0.41 ± 0.20**

All data represented as the mean ± standard deviation (SD)

** indicated significant difference ($p < 0.01$) between clinically healthy and non-metastatic lymph node.

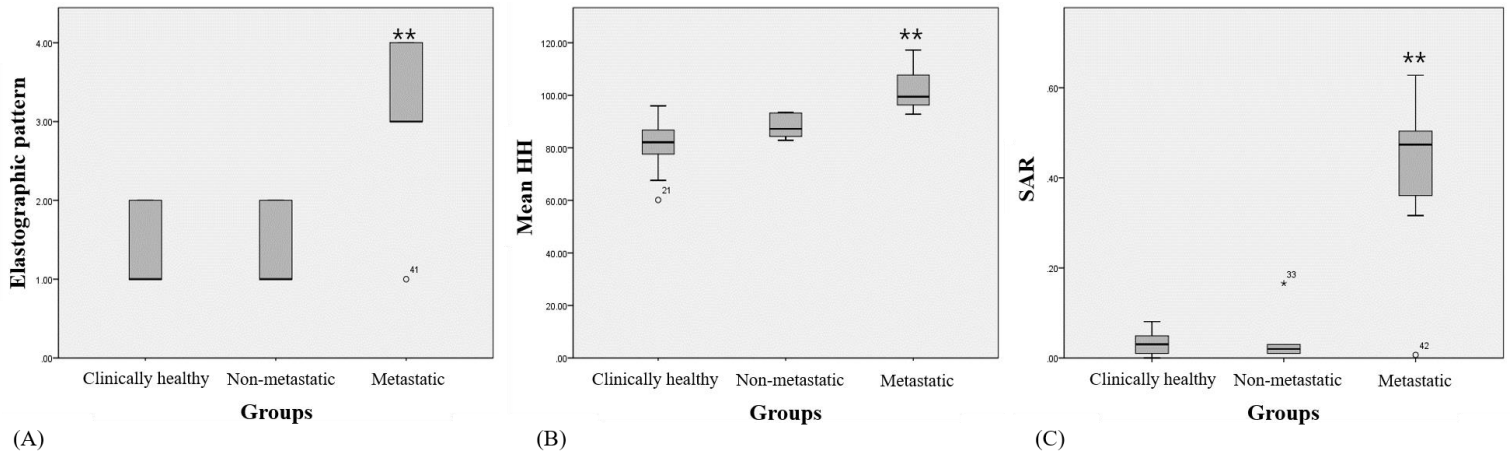

Figure 12. Box plot for elastographic pattern, mean hue histogram (mean HH) and stiffness area ratios (SAR) in different groups of lymph nodes (LN). Statistically significant in the elastographic pattern, hue histogram values and stiffness area ratio ($^{**}p < 0.01$) in metastatic LN compared to clinically healthy and non-metastatic LN.

Table 6. Diagnostic performance of B-mode and strain elastography in the predicting malignancy in mandibular lymph nodes.

	AUC	95% CI	*p* value	Cut-off	Sensitivity (%)	Specificity (%)	Youden Index
Mean hue histogram	0.982	0.878-1.000	<0.01	>92.26	100	91.89	0.92
Elastographic pattern	0.902	0.763-0.974	<0.01	>2	85.71	100	0.86
Stiffness area ratio	0.879	0.735-0.961	<0.01	>0.17	85.71	100	0.86
Width-to-depth ratio	0.661	0.492-0.804	0.1591	>0.48	57.14	77.50	0.35

AUC, Area under the curve

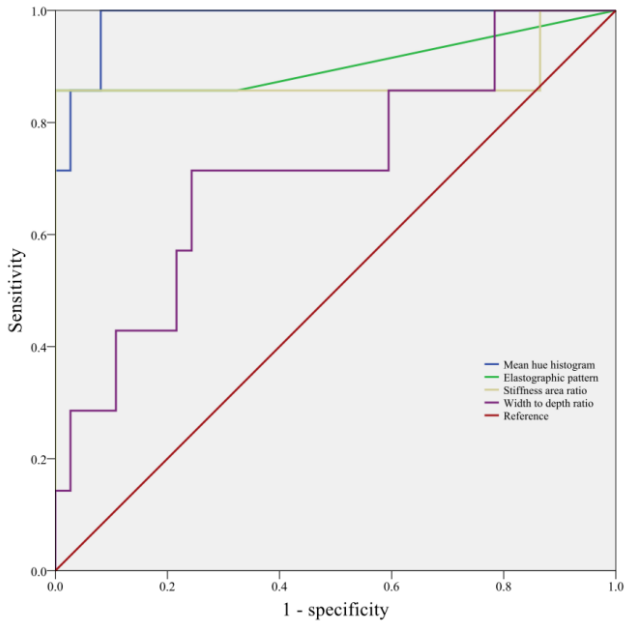

Figure 13. Receiver-operating characteristic curves assessing the diagnostic efficacy of grey scale ultrasonography and strain elastography for predicting mandibular lymph node malignancy. Area under the curve for mean hue histogram (0.982) is higher than those for elastographic pattern (0.902), stiffness area ratio (0.879) and width-to-depth ratio (0.661).

3. Lymphosonography

The sonographic features of the normal and patient groups are summarized in Table 7. After administering the perflubutane microbubbles by peritumoral injection, the dogs with head and neck cancer demonstrated simultaneous enhancement in the lymphatic vessels (n=3/11) and node (n=7/11) within 1 min and lasted 5 min post-injection and no efferent lymphatic vessels were not visualized in any patient. Four of the 5 non-metastatic nodes showed homogeneous enhancement patterns with centripetal filling in the mandibular lymph node (Figure 13), whereas the metastatic nodes showed focal (3/6, Figure 14B) or complete (3/6, Figure 14D) filling defects. The enhancement pattern and contrast enhancement intensity were significantly different between metastatic nodes and clinically healthy or non-metastatic nodes (p<0.05).

Table 7. Lymphosonographic findings in clinically healthy, non-metastatic and metastatic mandibular lymph nodes.

Variables			Clinically healthy (*n*=11)	Non-metastatic (*n*=5)	Metastatic (*n*=6)
Quantitative analysis	Visualization [a]	Lymphatic vessels	8	3	0
		Lymph node	11	4	3
	Lymphatic vessels diameter (mm) [b]		1.2 (0.7-1.8)	1.2 (1-1.4)	1(1)
	Contrast transit time (min) [b]	Lymphatic vessel	5 (5-7)	1(1)	1(1)
		Lymph node	5 (1-7)	1(1)	1(1)
	Lymph node enhancement mean intensity [b]		64.53 (24.81-128.43)	83.44 (72.57-139.70)	8.37 * (2.53-49.38)
Qualitative analysis	Lymph node enhancement pattern [a]	Completely filled	6	4	0
		Capsular filling	5	0	0
		Focal filling defect	0	0	3 *
		Full filling defect	0	1	3 *

[a] Data area expressed as number of dogs. [b] Data are expressed as median (range).

* indicated significant difference ($p < 0.05$) between clinically healthy and non-metastatic lymph node.

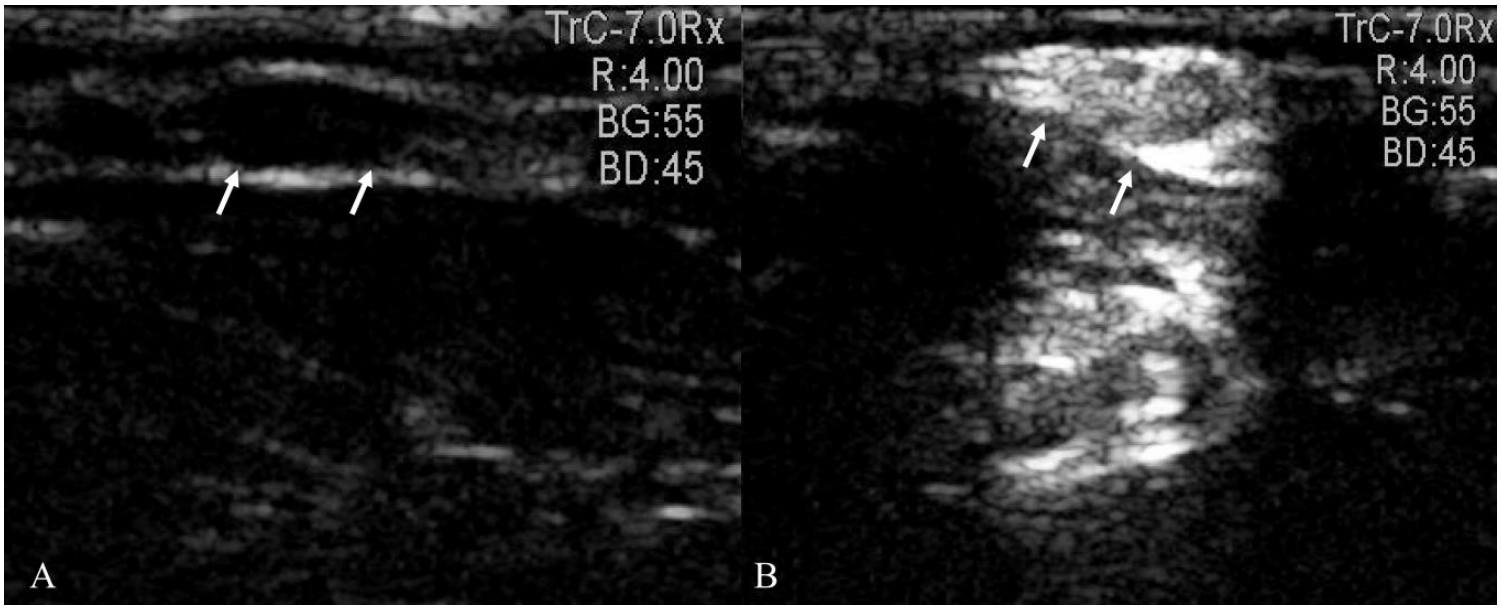

Figure 14. Image characteristics of non-metastatic lymph node contrast enhancement. On lymphosonography (A: pre-contrast, B: post-contrast), ipsilateral mandibular lymph node showing homogeneous enhancement (arrows). Primary cancer diagnosed as giant cell granuloma by histopathological examination, and cytology of the mandibular lymph node appearing normal.

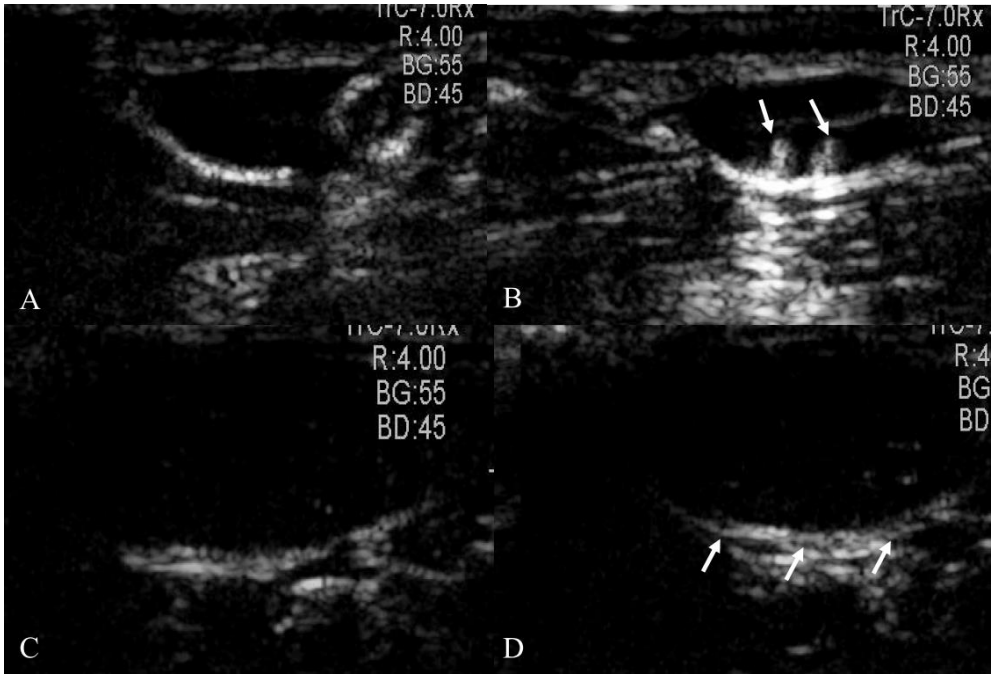

Figure 15. Image characteristics of a metastatic lymph node. On lymphosonography (A, C: pre-contrast, B, D: post-contrast), an ipsilateral mandibular lymph node showing a focal (B, arrows) or complete filling defect (D, arrows). Primary cancer diagnosed as melanoma (A, B) and adenocarcinoma (B, D) by histopathological examination and cytology of the mandibular lymph node showing metastasis.

4. Strain elastography combined with lymphosonography

One non-metastatic lymph node showed a full-filling defect on lymphosonography, but it showed a grade 1 elastographic pattern. In addition, one metastatic lymph node showed a grade 2 elastographic pattern, but it showed a full-filling defect on lymphosonography.

ROC analyses revealed that the best cutoff values for the prediction of metastatic lymph nodes were a score of 5 for the strain elastographic pattern ($p < 0.01$), with a sensitivity of 83.3% and specificity of 100%, a score of 5 for the lymphosonograhic contrast enhancement pattern ($p< 0.01$), with a sensitivity of 100% and specificity of 93.8%, and a score of 9 for combined evaluation ($p< 0.01$), with a sensitivity of 100% and specificity of 95%. Among the variables, combined evaluation showed the highest AUC of 0.999 (95% CI, 0.999-1.000).

DISCUSSION

Gray-scale ultrasonography is frequently used to assess lymph nodes in patients with cancer (Nyman HT and O'Brien RT 2007). Although the use of diagnostic criteria such as lymph node size, shape, parenchymal echogenicity, margination, and vascular pattern have been reported (Nyman *et al.,* 2005; Nyman *et al*., 2006; De Swarte M *et al*., 2011) the utility and specificity of these criteria for identifying metastatic lymph nodes remains unclear.

In the present study were evaluated the criteria of gray scale ultrasonography, strain elastography and lymphosonography. Although significant differences were observed in length-to-width ratios, most gray-scale ultrasonographic features, including width, parenchymal echogenicity, irregular margin, and hyperechoic hilum definition, were not significantly different. However, strain elastography and lymphosonography were significantly different between metastatic nodes and clinically healthy or non-metastatic nodes.

Strain elastography for predicting malignancy showed that most clinically healthy and non-metastatic lymph nodes had similar color patterns. In contrast, majority of metastatic lymph nodes were partially or substantially blue on elastograms which was probably related to their relative stiffness compared to the elasticity of the surrounding muscles and other anatomic structures. The reason why metastatic lymph nodes have a tendency to show higher tissue stiffness is associated with their altered tissue composition and structure. For metastatic lymph nodes, the cortex was damaged and thickened, and there was proliferation and cornification of

cancer cells. These alterations may produce keratin or fibrin in early stages before any morphological changes occur (Pereira *et al.,* 2015).

Elastographic patterns have been previously reported as superficial lymph node diagnostic criteria in veterinary medicine, which offered 80-100% sensitivity and 75-96% specificity (Belotta *et al*., 2019). However, no previous study has used semiquantitative strain elastography for predicting malignancy of mandibular lymph nodes. This previous experiment (chapter I) also found that elastographic patterns had high AUC values. However, this was relatively dependent on the examiner (k=0.53). Nevertheless, semiquantitative criteria, such as the mean hue histogram and stiffness area ratios, showed high repeatability and reproducibility, with the cutoff values for predicting malignancy being an elastographic pattern of >2, a mean hue histogram of > 92.26 and a stiffness area ratios of > 0.17.

The contrast enhancement pattern of lymphosonography makes prediction of lymph node status possible. Four of the five non-metastatic nodes showed completely filled enhancement similar to the clinically healthy group, whereas the metastatic nodes showed focal or complete filling defects. Many studies have reported that filling defects are significantly associated with tumor infiltration (Goldberg *et al.,* 2004; Lurie *et al.,* 2006; Curry *et al*., 2007). Tumor cells invade afferent lymphatic vessels and initially implant in the local cortical lymphoid sinus. With continued proliferation, tumor cells accumulate in the lymph nodes and obstruct or destroy the small lymphatic vessels, forming areas that do not enhance. Thus, the lymph node presents with heterogeneous enhancement. Moreover, contrast

transit time tended to be shorter in dogs with head and neck cancer. Lymph flow from tumors has been reported to be increased compared to that in normal tissue (Swartz and Lund, 2012). Increased lymph drainage has also been positively correlated with metastasis. (Pathak *et al*., 2006). Thus, lymphatic drainage from the tumor along with tumor recruitment of surrounding lymphatic vessels are likely to have important roles in modulating the immune response, with these manifesting as shorter contrast transit times.

Upon lymphonosography, capsular enhancement, which can be mistaken for a filling defect and thus misinterpreted as a metastatic lymph node, was observed in dogs of less one year old (n=4/5). This was likely due to their physiological status (i.e., extramedullary hematopoiesis), but additional histological confirmation is needed.

Analysis of the area under the ROC curve showed that the diagnostic power of the combined evaluation was higher than that of each individual evaluation. This suggests that examination can be best performed when lymphosonography, with its high sensitivity, and strain elastography, with its high specificity, are combined. One patient showed a normal strain elastography pattern (grade 1) but a complete filling defect on lymphosonography (combined score=10). We did not perform histopathologic examination, but the cause was suspected to be early stage metastasis. The combined method also reduced false-negative for diagnosing malignancy. However, one of the non-metastatic lymph nodes showed false-positive results for diagnosing malignancy using the combined method (combined score=12). Strain

elastography showed a normal elastographic pattern, but a complete filling defect on lymphosonography. This might be due to mechanical obstruction (Grimes *et al.,* 2017) as indicated by the lymph node's marked enlargement. Thus careful interpretation is necessary when severe lymphadenopathy is present since marked lymph node enlargement also occurs in metastatic lymph nodes.

The limitations of the present study include its inclusion of a small number of patients within each cytological diagnosis group for analyzing diagnostic performance. Given these findings, a large case-control study that incorporates a histologic conformation approach and includes variety of tumor types is required. Furthermore, clinically healthy dogs were selected based on clinical examination (physical examination, blood analysis and imaging studies) in order to avoid the use of invasive procedures, such as FNA or biopsy. Thus, it could not elucidate the homogeneity of the clinically healthy group.

In conclusion, semi-quantitative and qualitative strain elastography with high sensitivity may be helpful for pre-surgical prediction of mandibular lymph node malignancy in patients with head and neck cancer. Variables, such as the mean hue histogram and stiffness area ratio, which offer the highest diagnostic accuracy, can be used as aids to determine the need for further examinations such as FNA or biopsy. Furthermore, mandibular lymph nodes which showed filling defects after lymphosonography with high-grade strain elastographic patterns suggest metastasis in dogs with head and neck cancer. Thus this combination of lymphosonography and strain elastography is useful in predicting malignancy of lymph nodes.

CONCLUSION

The purpose of the present study was to predict mandibular lymph node malignancy using qualitative, semi-quantitative strain elastography and lymphosonography. Semi-quantitative and qualitative strain elastography with its high sensitivity and specificity, may be helpful for pre-surgical prediction of mandibular lymph node malignancy in patients with head and neck cancer. The cutoff values for predicting malignancy were an elastographic pattern >2, a mean hue histogram > 92.26 and stiffness area ratios > 0.17. Furthermore, the mandibular lymph nodes that showed a filling defect after lymphosonography highly suspected malignancy. However, when using strain elastography or lymphosonography alone, there were existed false positive or false negative findings. Therefore, this combination of lymphosonography and strain elastography is useful for predicting malignancy of lymph nodes.

GENERAL CONCLUSION

Strain elastography and lymphosonography are methods for evaluating mandibular lymph nodes that are non-invasive, simple, and easy to perform.

In clinically healthy dogs, mandibular lymph nodes exhibited predominantly red and green coloration on strain elastography. The semi-quantitative and qualitative variables, such as mean hue histogram, stiffness area ratio, and elastographic pattern exhibited no correlation with age and showed moderate to excellent repeatability/reproducibility. Lymphosonography showed direct visualization of the lymphatic vessels/mandibular lymph nodes. In normal mandibular lymph nodes, the afferent lymphatic vessels were visualized as hyperechoic linear structures leading from the injection site. Two enhancement patterns (capsular filling or completely filled) were observed.

In patients with head/neck cancer dogs, the non-metastatic lymph node showed a homogeneous green color (soft), the metastatic lymph node tended to be a heterogenous blue color (stiffer) on strain elastography. There was a significant difference ($p<0.01$) in the qualitative and quantitative criteria on strain elastographic criteria for the metastatic nodes compared to clinically healthy or non-metastatic nodes. For lymphosonography, clinically healthy and non-metastatic lymph nodes showed homogenous enhancement pattern with centripetal filling, whereas metastatic lymph nodes showed focal or complete filling defect. There was a significant difference ($p<0.05$) in contrast enhancement pattern in the metastatic nodes compared to clinical healthy or non-metastatic nodes.

Higher tissue stiffness (blue coloration) on strain elastography and filling defects on lymphosonography might be associated with altered tissue composition and structure of metastatic lymph nodes. The cortex was damaged and thickened with proliferation as well as cornification of cancer cells. These alterations may produce keratin/fibrin or destroy the small lymphatic vessels. Also, analysis of the area under the ROC curve showed that the diagnostic power of the combined evaluation was higher than that of each individual evaluation. This suggests that examination can be best performed when lymphosonography, with its high sensitivity, and strain elastography, with its high specificity, are combined.

In conclusion, filling defects after lymphosonography and high-grade strain elastographic patterns, may be helpful for pre-surgical malignancy prediction in patients with head and neck cancer dogs. However, when using strain elastography or lymphosonography alone, there were existed false positive or false negative findings so that the combination of lymphosonography and strain elastography is recommended for predicting malignancy of lymph nodes.

REFERENCES

Alam F, Naito K, Horiguchi J, Fukuda H, Tachikake T, Ito K. Accuracy of sonographic elastography in the differential diagnosis of enlarged cervical lymph nodes: comparison with conventional B-mode sonography. AJR Am J Roentgenol, 2008; 191: 604-610.

Ballegeer EA, Adams WM, Dubielzig RR, Paoloni MC, Klauer JM, Keuler NS. Computed tomography characteristics of canine tracheobronchial lymph node metastasis. Vet Radiol Ultrasound, 2010; 51: 397-403.

Barr RG. Real-time ultrasound elasticity of the breast: initial clinical results. Ultrasound Q, 2010; 26: 61–66.

Barr RG, Zhang Z. Effects of precompression on elasticity imaging of the breast: development of a clinically useful semiquantitative method of precompression assessment. J Ultrasound Med, 2012; 31: 895-902.

Beer P, Pozzi A, Rohrer-Bley C, Bacon N, Pfammatter NS, Venzin C. The role of sentinel lymph node mapping in small animal veterinary medicine: A comparison with current approaches in human medicine. Vet Comp Oncol. 2018; 16: 178-187.

Belotta AF, Gomes MC, Rocha NS, Melchert A, Gluffrida R, Silva JP, Mamprim MJ. Sonography and sonoelastography in the detection of malignancy in superficial lymph nodes of dogs. J Vet Intern Med, 2019; 33: 1403-1413.

Bhatia KS, Cho CC, Yuen YH, Rasalkar DD, King AD, Ahuja AT. Real-time qualitative ultrasound elastography of cervical lymph nodes in routine clinical practice: interobserver agreement and correlation with malignancy. Ultrasound Med Biol, 2010; 36: 1990-1997.

Blomley MJ, Albrecht T, Cosgrove DO, Patel N, Jayaram V, Butler-Barnes J, Eckersley RJ, Bauer A, Schlief R, Improved imaging of liver metastases with stimulated acoustic emission in the late phase of enhancement with the US contrast agent SH U 508A: early experience. Radiology, 1999; 210: 409-416.

Boston SE, Lu X, Culp WTN, et al. Efficacy of systemic adjuvant therapies administered to dogs after excision of oral malignant melanomas: 151 cases (2001-2012). J Am Vet Med Assoc, 2014; 245: 401-407.

Brissot HN, Edery DG. Use of indirect lymphography to identify sentinel lymph node in dogs: a pilot study in 30 tumours. Vet Comp Oncol, 2017; 15: 740-753.

Burnside ES, Hall TJ, Sommer AM, Hesley GK, Sisney GA, Svensson WE, Fine JP, Jiang J, Hangiandreou NJ. Differentiating benign from malignant solid breast masses with US strain imaging. Radiology, 2007; 245: 401–410.

Carlsen JF, Ewertsen C, Sletting S, Talman ML, Vejborg I, Bachmann Neilsen M. Strain histograms are equal to strain ratios in predicting malignancy in breast tumours. PLoS One, 2017; 12: e0186230.

Chiorean L, Barr RG, Braden B, Jenssen C, Cui XW, Hocke M, Schuler A, Dietrich CF. Transcutaneous Ultrasound: Elastographic Lymph Node Evaluation. Current Clinical Applications and Literature Review. Ultrasound Med Biol, 2016; 42: 16-30.

Ciekot PA, Powers BE, Withrow SJ, Straw RC, Ogilvie GK, Larue SM. Histologically low-grade, yet biologically high-grade, fibrosarcomas of the mandible and maxilla in dogs: 25 cases (1982-1991). J Am Vet Med Assoc, 1994; 204: 610-615.

Cowell, R.L., Dorsey, K.E., Meinkoth, J.H., 2003. Lymph node cytology. Veterinary Clinics of North America: Small Animal Practice 33, 47-67.

Culp WTN, Ehrhart N, Withrow SJ, et al. Results of surgical excision and evaluation of factors associated with survival time in dogs with lingual neoplasia: 97 cases (1995-2008). J Am Vet Med Assoc, 2013; 242: 1392-1397.

Curry JM, Bloedon E, Malloy KM, Cognetti DM, Merton DA, Goldberg BB, Keane WM, Rosen D, Pribitkin EA. Ultrasound-guided contrast-enhanced sentinel node biopsy of the head and neck in a porcine model. Otolaryngol Head and Neck Surg, 2007; 137: 735-741.

De Swarte M, Alexander K, Rannou B, D'Anjou MA, Blond L, Beauchamp G. Comparison of sonographic features of benign and neoplastic deep lymph nodes in dogs. Vet Radiol Ultrasound, 2011; 52: 451-456.

Desmots F, Fakhry N, Mancini J, Reyre A, Vidal V, Jacquier A, Santini L, Moulin G, Varoquaux A. Shear wave elastography in head and neck lymph node assessment: image quality and diagnostic impact compared with B-mode and Doppler ultrasonography. Ultrasound Med Biol, 2016; 42: 387-398.

Dietrich CF, Barr RG, Farrokh A, Dighe M, Hocke M, Jenssen C, Dong Y, Saftoiu A, Havre RF. Strain Elastography - How To Do It? Ultrasound Int Open, 2017; 3: E137-E149.

Dietrich CF, Cantisani V. Current status and perspectives of elastography. Eur J Radiol, 2014; 83: 403-404.

Favril S, Stock E, Hernot S, Hesta M, Polis I, Vanderperren K, de Rooster H. Sentinel lymph node mapping by near-infrared fluorescence imaging and contrast-enhanced ultrasound in healthy dogs. Vet Comp Oncol, 2019; 17: 89-98.

Fulton AJ, Nemec A, Murphy BG, Kass PH, Verstraete FJM. Risk factors associated with survival in dogs with nontonsillar oral squamous cell carcinoma 31 cases (1990-2010). J Am Vet Med Assoc, 2013; 243: 696-702.

Gelb HR, Freeman LJ, Rohleder JJ, Snyder PW. Feasibility of contrast-enhanced ultrasound-guided biopsy of sentinel lymph nodes in dogs. Vet Radiol Ultrasound. 2010; 51: 628-633.

Gieger TL, Théon AP, Werner JA, McEntee MC, Rassnick KM, DeCock HEV. Biologic behavior and prognostic factors for mast cell tumors of the canine muzzle: 24 cases (1990-2001). J Vet Intern Med, 2003; 17: 687-692.

Goldberg BB, Merton DA, Liu JB, Forsberg F, Zhang K, Thakur M, Schulz S, Schanche R, Murphy GF, Waldman SA. Contrast-enhanced ultrasound imaging of sentinel lymph nodes after peritumoral administration of Sonazoid

in a melanoma tumor animal model. J Ultrasound Med, 2011; 30: 441-453.

Goldberg BB, Merton DA, Liu JB, Murphy G, Forsberg F. Contrast-enhanced sonographic imaging of lymphatic channels and sentinel lymph nodes. J Ultrasound Med, 2005; 24: 953-965.

Goldberg BB, Merton DA, Liu JB, Thakur M, Murphy GF, Needleman L, Tornes A, Forsberg F. Sentinel lymph nodes in a swine model with melanoma, contrast-enhanced lymphatic US. Radiology, 2004; 230: 727-734.

Grimes JA, Secrest SA, Northrup NC, Saba CF, Schmiedt CW. Indirect computed tomography lymphangiography with aqueous contrast for evaluation of sentinel lymph nodes in dogs with tumors of the head. Vet Radiol Ultrasound, 2017; 58: 559-564.

Herring ES, Smith MM, Robertson JL. Lymph node staging of oral and maxillofacial neoplasms in 31 dogs and cats. J Vet Dent, 2002; 19: 122-126.

Ikomi F, Kawai Y, Ohhashi T. Recent advance in lymph dynamic analysis in lymphatics and lymph nodes. Ann Vasc Dis, 2012; 5: 258-268.

Itoh A, Ueno E, Tohno E, Kamma H, Takahashi H, Shiina T, Yamakawa M, Matsumura T. Breast Disease: Clinical Application of US Elastography for Diagnosis. Radiology, 2006; 239: 341–350.

Johnson PJ, Elders R, Pey P, Dennis R. Clinical and magnetic resonance imaging features of inflammatory versus neoplastic medial retropharyngeal lymph node mass lesions in dogs and cats. Vet Radiol Ultrasound, 2016; 57: 24-32.

Kanemoto H, Ohno K, Nakashima K, Takahashi M, Fujino Y, Nishimura R, Tsujimoto H. Characterization of canine focal liver lesions with contrast-enhanced ultrasound using a novel contrast agent-sonazoid. Vet Radiol Ultrasound, 2009; 50: 188-194

Langenbach A, McManus PM, Hendrick MJ, Shofer FS, Sorenmo KU. Sensitivity and specificity of methods of assessing the regional lymph nodes for evidence of metastasis in dogs and cats with solid tumors. J Am Vet Med Assoc, 2001; 218: 1424-1428.

Lee SH, Cho N, Chang JM, Koo HR, Kim JY, Kim WH, Bae MS, Yi A, Moon WK. Two-view versus single-view shear-wave elastography: comparison of observer performance in differentiating benign from malignant breast masses. Radiology, 2014; 270: 344–353.

Liu JB, Merton DA, Berger AC, Forsberg F, Witkiewicz A, Zhao H, Eisenbrey JR, Fox TB, Goldberg BB. Contrast-enhanced sonography for detection of secondary lymph nodes in a melanoma tumor animal model. J Ultrasound Med. 2014; 33: 939-947.

Lurie DM, Seguin B, Schneider PD, Verstraete FJ, Wisner ER. Contrast-assisted ultrasound for sentinel lymph node detection in spontaneously arising canine head and neck tumors. Invest Radiol, 2006; 41: 415-421.

Lyshchik A, Higashi T, Asato R, Tanaka S, Ito J, Hiraoka M, Insana MR, Brill AB, Saga T, Togashi K. Cervical lymph node metastases: diagnosis at sonoelsatography-initial experience. Radiology 2007; 243: 258-267.

Macdonald AJ, Arkill KP, Tabor GR, McHale NG, Winlove CP. Modeling flow in collecting lymphatic vessels: one-dimensional flow through a series of contractile elements. Am J Physiol Heart Circ Physiol, 2008; 295: H305-313.

Matsuzawa F, Omoto K, Einama T, Abe H, Suzuki T, Hemaguchi J, Kaga T, Sato M, Oomura M, Takata Y. Accurate evaluation of axillary sentinel lymph node metastasis using contrast enhanced ultrasonography with Sonazoid in breast cancer: a preliminary clinical trial. Springerplus. 2015;4: 509.

Moon WK, Choi JW, Cho N, Park SH, Chang JM, Jang M, Kim KG. Computer-aided analysis of ultrasound elasticity images for classification of benign and malignant breast masses. AJR Am J Roentgenol, 2010; 195: 1460-1465.

Nakajima T, Inage T, Sata Y, Morimoto J, Tagawa T, Suzuki H, Iwata T, Yoshida S, Nakatani Y, Yoshino I. Elastography for Predicting and Localizing Nodal Metastases during Endobronchial Ultrasound. Respiration, 2015; 90: 499-506.

Nakamura K, Takagi S, Sasaki N, Bandula Kumara WR, Murakami M, Ohta H, Yamasaki M, Takiguchi M. Contrast-enhanced ultrasonography for characterization of canine focal liver lesions. Vet Radiol Ultrasound, 2010; 51: 79-85

Nielsen KR, Grossjohann HS, Hansen CP, Nielsen MB. Use of contrast-enhanced ultrasound imaging to detect the first draining lymph node (FDLN) in a swine model: correlation of imaging findings with the distance from the injection site to the FDLN. J Ultrasound Med. 2008; 27: 1203-1209.

Nyman HT, O'Brien RT. The sonographic evaluation of lymph nodes. Clin Tech Small Anim Pract, 2007; 22: 128-137.

Nyman HT, Kristensen AT, Skovgaard IM, McEvoy FJ. Characterization of normal and abnormal canine superficial lymph nodes using gray-scale B-mode, color flow mapping, power, and spectral Doppler ultrasonography: a multivariate study. Vet Radiol Ultrasound, 2005; 46: 404-410.

Nyman HT, Lee MH, McEvoy FJ, Nielsen OL, Martinussen T, Kristensen AT. Comparison of B-mode and Doppler ultrasonographic findings with histologic features of benign and malignant superficial lymph nodes in dogs. Am J Vet Res, 2006; 67: 978-984.

Ophir J, Céspedes I, Ponnekanti H, Yazdi Y, Li X. Elastography: a quantitative method for imaging the elasticity of biological tissues. Ultrason Imaging, 1991; 13: 111-134.

Ozturk A, Grajo JR, Dhyani M, Anthony BW, Samir AE. Principles of ultrasound elastography. Abdom Radiol (NY), 2018; 43: 773-785.

Pathak AP, Artemov D, Neeman M, Bhujwalla ZM. Lymph node metastasis in breast cancer xenografts is associated with increased regions of extravascular drain, lymphatic vessel area, and invasive phenotype. Cancer Res, 2006; 66: 5151-5158.

Pereira ER, Jones D, Jung K, Padera TP. The lymph node microenvironment and its role in the progression of metastatic cancer. Semin Cell Dev Biol, 2015; 38: 98-105

Preucil F, "Color Hue and Ink Transfer- Their Relation to Perfect Reproduction, *TAGA Proceedings,* 1953, 102-110.

Proulx DR, Ruslander DM, Dodge RK, Hauck ML, Willams LE, Horn B, Price GS, Thrall DE. A retrospective analysis of 140 dogs with oral melanoma treated with external beam radiation. Vet Radiol Ultrasound, 2003; 44: 352-359.

Regner DM, Hesley GK, Hangiandreou NJ, Morton MJ, Nordiand MR, Meixner DD, Hall TJ, Farrell MA, Mandrekar JN, Harmsen WS, Charboneau JW. Breast lesions: evaluation with US strain imaging—clinical experience of multiple observers. Radiology, 2006; 238: 425–437.

Seiler GS, Griffith E. Comparison between elastographic stiffness scores for benign versus malignant lymph nodes in dogs and cats. Vet Radiol Ultrasound, 2018; 59: 79-88.

Sever AR, Mills P, Jones SE, Mali W, Jones PA. Sentinel node identification using microbubbles and contrast-enhanced ultrasonography. Clin Radiol, 2012; 67:

687-694.

Shiina T, Nightingale KR, Palmeri ML, Hall TJ, Bamber JC, Barr RG, Castera L, Choi BI, Chou YH, Cosgrove D et al. WFUMB Guidelines and Recommendations for Clinical Use of Ultrasound Elastography: Part 1: Basic Principles and Terminology. Ultrasound in Medicine & Biology, 2015; 41:1126–1147.

Sigrist RMS, Liau J, Kaffas AE, Chammas MC, Willmann JK. Ultrasound Elastography: Review of Techniques and Clinical Applications. Theranostics, 2017; 7:1303–1329.

Sinem K, Michael D. Mechanism of lymphatic metastasis. J Clin Invest. 2014; 124: 922-928.

Stahle JA, Larson MM, Rossmeisl JH, Dervisis N, Neelis D. Diffusion weighted magnetic resonance imaging is a feasible method for characterizing regional lymph nodes in canine patients with head and neck disease. Vet Radiol Ultrasound 2018; 60: 176-183.

Swartz MA, Lund AW. Lymphatic and interstitial flow in the tumour microenviroment: linking mechanobiology with immunity. Nat Rev cancer,

2012; 12: 210-219.

Tan R, Xiao Y, He Q. Ultrasound elastography: its potential role in assessment of cervical lymphadenopathy. Acad Radiol, 2010; 17: 849-855.

Theon AP, Rodriguez C, Madewell BR. Analysis of prognostic factors and patterns of failure in dogs with malignant oral tumors treated with megavoltage irradiation. J Am Vet Med Assoc, 1997; 210: 778-784.

Thomas A, Kümmel S, Fritzsche F, Warm M, Ebert B, Hamm B, Fischer T. Real time sonoelastography performed in addition to B-mode ultrasound and mammography: improved differentiation of breast lesions? Acad Radiol, 2006; 13: 1496–1504.

Tuohy JL, Milgram J, Worley DR, Dernell WS. A review of sentinel lymph node evaluation and the need for its incorporation into veterinary oncology. Vet Comp Oncol. 2009;. 7: 81-91.

Viera AJ, Garrett JM. Understanding interobsever agreement: the kappa statistic. Fam Med, 2005; 37: 360-363.

Williams LE, Packer RA. Association between lymph node size and metastasis in dogs with oral malignant melanoma: 100 cases (1987-2001). J Am Vet Med Assoc, 2003; 222: 1234-1236.

Wojcinski S, Dupont J, Schmidt W, Cassel M, Hilemanns P. Real-time ultrasound elastography in 180 axillary lymph nodes: Elasticity distribution in healthy lymph nodes and prediction of breast cancer metastases. BMC Med Imaging, 2012; 12: 35.

Zhou J, Zhou C, Zhan W, Jia X, Dong Y, Yang Z. Elastography ultrasound for breast lesions: fat-to-lesion strain ratio vs gland-to-lesion strain ratio. Eur Radiol, 2014; 24: 3171–3177.

국 문 초 록

두경부 종양 개에서 탄성 초음파 및 초음파 림프조영을 이용한 하악 림프절 평가의 임상적 유용성

최 미 현

지도교수 최 민 철

서울대학교 대학원

수의학과 임상수의학 전공

종양 환자에서 림프절 전이 여부는 환자의 병기 진단 및 치료 계획 수립에 있어 중요하여 그간 다양한 종류의 영상 검사를 통한 평가 방법이 논의되었다. 하지만 대부분 양성과 악성의 기준이 모호한 결과를 보

여 세포/조직 검사 전 간단하게 시행할 수 있는 새로운 림프절 평가 방법이 필요하다.

최근 새로운 림프절 평가 방법으로 초음파 조영 검사와 탄성 초음파 검사가 고안되었다. 초음파 조영 검사는 실질 조직 내 조영제를 주입하여 림프계통을 영상화 하고, 탄성 초음파는 일반적인 종양 세포의 경도가 높아짐을 영상학적으로 시각화 한 방법으로, 수의에서 이 두가지 방법을 이용한 경부 림프절 평가의 진단적 가치에 대해 명확하게 보고되지 않았다. 따라서 본 실험의 목적은 임상적으로 건강한 개에서 정량 및 정성적인 분석을 통한 초음파 탄성 검사 (제 1장) 및 초음파 림프 조영 검사 (제 2장)의 정상 영상 특징을 확인하고, 이를 두경부 종양 환자에 적용하여 각 방법의 유용성을 알아보는 것이다 (제 3장).

제 1장에서는 총 45마리의 임상적으로 건강한 개체에서, 초음파 탄성 영상을 정성 및 정량적으로 분석하였다. 정성적인 방법은 탄성영상 패턴 (림프절 내 단단한 부분이 차지하는 범위를 1에서 4점으로 나누어 평가)을 분석하고 정량적인 방법은 평균 휴 히스토그램 값 (mean hue histogram value: 전체 림프절 내 평균 pixel 값)과 강성도 면적 범위율 (stiffness area ratio)을 Image J 프로그램을 통해 분석하였다. 정상 하악 림프절은 초음파 탄성 영상에서 주로 적색에서 녹색으로 표현되며, 탄성 패턴은 1점 혹은 2점으로 평가 (1.23 ± 0.42, 평균 ± 표준편차) 되었다. 평균 휴 히스토그램 (80.96 ± 8.29), 강성도 면적 범위율 (0.03 ±

0.02) 및 탄성 패턴은 개체의 나이와 상관관계를 보이지 않으며, 관찰자 간/ 관측자 내 일치도는 중등도 이상 확인되었다.

제 2장에서는 총 11마리의 임상적으로 건강한 개체에서, 초음파 림프 조영 영상을 정성 및 정량적으로 분석하였다. 정성적인 방법은 조영 증강 패턴 (전체 조영, 껍질 조영, 부분 충진 결손, 완전 충진 결손)을, 정량적인 방법은 림프절/림프관의 영상화 여부 및 조영제 이행 시간 (조영제 주입 후 림프관/림프절이 영상화 되는데까지 걸리는 시간), 조영 증강 정도 (Image J)를 평가하였다. 구강 점막 내로 조영제 (Sonazoid®) 1*ml* 주입 후 정상 수입 림프관은 조영제 주입 후 5분, 하악 림프절은 수입 림프관과 동시에 영상화 되어 10분째까지 영상화가 지속되었다. 수입 림프관은 고에코의 관상 구조 (직경: 1.2 *mm*) 로 확인되며, 이는 동방향의 하악 림프절로 연결되고 하악 림프절 중간값 조영 증강 정도는 64.53 (범위: 24.81-128.43)으로 껍질성 혹은 전반적인 균일한 조영증강을 보였다. 초음파 림프 조영 검사는 정상 개체의 림프 순환 (수입 림프관, 하악 림프절)을 실시간으로 영상화 할 수 있는 장점이 확인되었다.

제 3장에서는 두경부 종양 환자에서 초음파 탄성 검사 (21개 림프절, 비 전이=8개, 전이=13개)과 초음파 림프 조영 검사 (11마리, 비 전이=5마리, 전이=6마리)을 적용하여 임상적으로 건강한 개체 (초음파 탄성 검사: 45마리, 초음파 림프 조영: 11마리)와 비교 분석하였다. 초음파 탄성 검사에서 임상적으로 건강한 개체 (45/45)와 비 전이성 (1/8) 하악 림프

절은 균일한 녹색 양상을 보였으나, 전이성 (12/13) 하악 림프절은 이질적이고 청색 양상으로 확인되었다. 또한 전이성 림프절은 임상적으로 건강한 개체와 비 전이성 하악 림프절과 비교하여 정성적인 기준과 정량적인 기준 모두 통계적으로 유의한 차이를 보였고, 악성 림프절 예측값은 평균 휴 히스토그램은 92.26 (민감도: 100%, 특이도 92%), 강성도 면적 범위율은 0.17 (민감도: 85%, 특이도 100%)로 계산되었다. 초음파 림프조영 검사에서 임상적으로 건강한 개체 (11/11)와 비 전이성 (4/5) 하악 림프절은 균일한 구심성의 조영 증강을 보였으나, 전이성 하악 림프절의 경우 국소적인 (3/6) 혹은 전체적인 (3/6) 조영제 충진 결손을 보였으며 전이성 림프절은 임상적으로 건강한 개체와 비 전이성 하악 림프절과 비교하여 정성적인 기준과 정량적인 기준 모두 통계적으로 유의한 차이를 나타냈다. 또한 각 검사의 단일 수행 보다는 혼합 방법 분석이 가장 높은 곡선 아래 면적 값을 보였다. 이는 림프절 전이 시 림프계통 변화 (림프계 혈관 신생으로 인한 림프절 실질 내 케라틴, 섬유소 등의 증가) 및 림프절 피질 내 직접적인 전이성 조직 침습으로 인해 탄성도가 감소 (강성도 증가) 및 조영 검사에서의 충진 결손으로 나타난 것으로 판단된다.

결론적으로, 정성 및 정량적인 초음파 탄성 검사 및 초음파 조영 검사는 악성 림프절 선행 평가에 유용하며, 초음파 탄성 검사에서의 강성도 증가 및 초음파 림프절 조영 검사 후 조영제 충진 결손은 전이성 림

프절을 의심할 수 있는 소견이다. 다만, 초음파 탄성 혹은 초음파 림프절 조영 단독 검사 시 위 양성 혹은 위 음성 진단 가능성이 있는 바 두 가지 검사의 혼합 방법이 추천된다.

주요어: 개, 두경부 종양, 하악 림프절, 소나조이드, 초음파 림프 조영 검사, 반정량 탄성 초음파,

학번: 2015-31181